HUBBLE TENSION IN THE CONTEXT OF COSMOLOGICAL SCALAR FIELD MODELS

A Thesis Submitted to
the Graduate School of
İzmir Institute of Technology
in Partial Fulfillment of the Requirements for the Degree of

MASTER OF SCIENCE

in Physics

by
Rand Abdel Latif Suleiman ALFAR

March 2024
İZMİR

We approve the thesis of **Rand Abdel Latif Suleiman ALFAR**

Examining Committee Members:

Prof. Dr. Recai ERDEM
Supervisor, Department of Physics, İzmir Institute of Technology

---

Prof. Dr. Kadri YAKUT
Department of Astronomy and Space Sciences, Ege University

Asst. Prof. Dr. Heeseung Zoe
Department of Physics, İzmir Institute of Technology

29 March 2024

Prof. Dr. Lütfi ÖZYÜZER
Head of the Department of
Physics

Prof. Dr. Mehtap EANES
Dean of the Graduate School

Dedicated to my mother, my father, my fiance, and my siblings.....

ACKNOWLEDGMENTS

I would like to take this opportunity to express my deep appreciation and gratitude to my supervisor, Prof. Dr. Recai ERDEM, for his invaluable guidance, constant support, and generous allocation of time throughout the completion of my master's thesis. His unwavering assistance, kindness, availability, and encouragement have played a pivotal role in the successful completion of this research endeavor. It has been an absolute pleasure to work under his supervision, and I am truly grateful for his mentorship.

I would also like to extend my gratitude to Prof. Dr. Kadri YAKUT and Asst. Prof. Dr. Heeseung Zoe for their participation as jury members and for engaging in insightful discussions regarding my thesis. I am sincerely grateful for the opportunity to engage in fruitful discussions with them.

I would also like to express my gratitude to my dear friends from around the world for their unwavering support, encouragement, and friendship. Their presence and continuous motivation have made my journey more enjoyable and fulfilling. I am truly fortunate to have such amazing friends in my life.

Furthermore, I am eternally grateful to my beloved family and my fiance for their unconditional love, unwavering support, and constant encouragement. Their belief in me and their selfless sacrifices have been the driving force behind my accomplishments. I am incredibly fortunate to have them by my side, and I am forever indebted to them for their immeasurable contributions.

Lastly, I would like to extend my gratitude to all those who have directly or indirectly contributed to the completion of this thesis. Your support, encouragement, and belief in my abilities have been invaluable and deeply appreciated.

ABSTRACT

HUBBLE TENSION IN THE CONTEXT OF COSMOLOGICAL SCALAR FIELD MODELS

This thesis delves into the issue of Hubble tension that is the discrepancy between different types of measurements of the expansion rate of the universe at present (i.e. Hubble constant H_0). Various techniques can be employed to measure H_0. There are two types of measurements, namely, direct and indirect measurements for measurement of H_0. Direct measurements involve determining the recession velocities of galaxies or supernovae at relatively small cosmological distances, so this type of measurements are direct local measurements. On the other hand, indirect measurements encompass both local methods, such as utilizing the Tully-Fisher relation, and non-local approaches, including cosmic microwave background (CMB) measurements and baryon acoustic oscillation (BAO) measurements of large-scale structures (LSS). The most precise local measurements are achieved through supernovae calibrated by Cepheid variable star measurements, while CMB measurements provide the most precise non-local measurements. However, even when considering measurement errors, there is a significant discrepancy between supernovae and CMB measurements. This is known as the Hubble tension. A milder discrepancy is also observed between local direct measurements and BAO measurements. Many different potential sources of this tension and many different models are proposed to resolve this tension. This thesis focuses on the subset of the proposed models that employ scalar fields in the context of general relativity. The primary objective is to provide a comprehensive understanding of the fundamental ideas underlying these models and emphasize their theoretical aspects.

ÖZET

KOZMOLOJİK SKALAR ALAN MODELLERİ KAPSAMINDA HUBBLE GERİLİMİ

Bu tez, evrenin günümüzdeki genişleme hızını ölçmek için kritik bir parametre olan Hubble sabitinin, H_0'un ölçüm sonuçlarındaki büyük farklılıklara odaklanmaktadır. H_0'u ölçmek için çeşitli teknikler kullanılabilir ve bunlar genel olarak doğrudan ve dolaylı ölçümler olarak kategorize edilebilirler. Doğrudan ölçümler, galaksilerin veya süpernovaların göreceli küçük kozmik mesafelerdeki uzaklaşma hızlarının belirlenmesini içerir, bu nedenle bu tip ölçümler doğrudan yerel ölçümlerdir. Öte yandan, dolaylı ölçümler, Tully-Fisher ilişkisi gibi lokal yöntemleri ve kozmik mikrodalga arka plan (CMB) ölçümleri ve büyük ölçekli yapıların baryon akustik osilasyon (BAO) ölçümlerini içeren lokal olmayan yaklaşımları kapsar. En hassas yerel ölçümler, Cepheid değişken yıldız ölçümleri tarafından kalibre edilen süpernova ölçümleriyle elde edilirken, CMB ölçümleri en hassas olmayan lokal olmayan ölçümleri sağlar. Bununla birlikte, ölçüm hataları dikkate alındığında bile, süpernova ve CMB ölçümleri arasında önemli bir uyuşmazlık, Hubble gerilimi olarak bilinen bir farklılık ortaya çıkar. Yerel doğrudan ölçümler ile BAO ölçümleri arasında daha hafif bir farklılık olsa da yine de farklılık belirgindir. Literatürde, bu gerilimin çözümü için birçok farklı potansiyel neden ve model önerilmektedir. Bu tez, genel görelilik çerçevesinde skalar alanlar kullanan modellerin bir alt kümesine odaklanmaktadır. Temel hedef, bu modellerin temel fikirlerinin kapsamlı bir anlayışını sağlamak ve önemli teorik yönlerini vurgulamaktır.

TABLE OF CONTENTS

LIST OF FIGURES

CHAPTER 1

INTRODUCTION

In 1929 Edwin Hubble observed that the galaxies at cosmological distances are receding from Earth and their recession speeds are proportional to their distances [44]. This verified the predictions obtained by Alexander Friedmann in 1922 [36] and independently by Georges Lemaitre in 1927 [54]. The expansion rate of the universe is described by the Hubble constant H_0 which expresses how many times a given physical distance in the universe increases in a unit of time. The standard unit for H_0 is km/ Mpc /s where Mpc $= 3.1 \times 10^{16}$ km. In fact, it is also used to determine the age and the composition of the universe in the standard model of cosmology [97]. Since its introduction, H_0 has been measured many times at different times [29, 49, 51, 66]. The first observational result was of the order of 500 km/ Mpc /s [44], but the uncertainty was large.Then, for decades the H_0 was measured between 50 and 100 km/ Mpc /s [19, 34, 89] Even in 1994, its value was in the range of 61 - 85 km/Mpc/s by observations of supernovas [83]. In recent years H_0 has been also measured by studying cosmic microwave background (CMB) radiation in the context of the standard model of cosmology that is called Λ-Cold-Dark-Matter (ΛCDM). Then, it has been noticed that the value of H_0 measured from CMB is significantly smaller than the direct measurements of the recession speeds of the galaxies and supernovas at cosmological distances. However, the first measurements were compatible with the direct measurements within the error bars. However, the disagreement between these two methods turned into tension after improvements in the error bars in the direct measurements. Now the disagreement between the direct measurements and CMB measurements are more than 5σ[1] [47]. This is called Hubble tension. See Fig. 1.1.

There are many proposals for the solution of the Hubble tension [10, 12, 16, 17, 20, 26, 28, 59, 72]. At first, some systematic errors were thought to be the source of the

[1] σ is used to designate one standard deviation in a Gaussian distribution. In general, a "5 sigma" deviation, plus or minus, indicates how far out on the distribution you are from the mean. The departure from the mean value in such a distribution is commonly expressed in terms of the number of standard deviations. Here, as we have two independent measurements and the uncertainties follow a roughly normal distribution, 5 sigma indicates that the difference between the two values is 5 times the expected standard deviation of the difference between the two numbers.

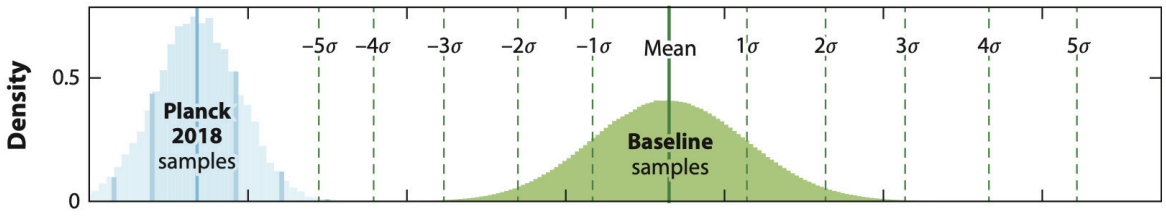

Figure 1.1. 5σ confidence level can be shown by the extended Markov chain Monte Carlo sampling of the posterior for the Hubble constant H_0. where the Planck Collaboration chains (blue) and the Supernovae and H_0 for the Equation of State (SH0ES) Collaboration (green) provide the probability density for the baseline [47]

tension. But studies show that this is not the case [29, 42, 45, 76, 78, 95], especially after the measurements have gotten more and more precise with 8σ Confidence level [77]. There are different assumptions and models for the solution of the tension by the inclusion of new physics. Some models adopt the approach that the missing physics is due to gravitational physics. This type of models modify the gravitational part of physics, for example [37]. Other type of models assume that general relativity is valid at all scales while the source term of the Einstein equations, or the Robertson-Walker metric [60] is modified. Typically, there are two types of such models; late time solutions and early time solutions. Late time solutions modify the standard model after recombination era [2] while early time solutions modify it just before the recombination.

In this thesis we adopt the second approach above i.e. we consider the models that modify the matter and energy content of the standard model. There are different kinds of models of this type. Some of them, modify the matter content in an ad hoc and phenomenological way [2, 55, 57] while others add new cosmological fields, such as scalars, vector fields, fermions, etc. In this thesis, we limit ourselves to scalar field models.

[2] which happened around 380,000 years after the Big Bang and is the period in the early universe when electrons and protons combined to form neutral atoms, and the photons were allowed to flee the hot, dense plasma of the universe and travel freely resulting cosmic microwave background radiation (CMB)

CMB measurements of Hubble constant assume the standard model of cosmology. Therefore, in the next chapter, we give a brief overview of the standard model. In Chapter 3 we briefly consider the basic distance measurement techniques at small redshifts and cosmic distance ladder that is essential for the direct measurements of Hubble constant. In Chapter 4 the basic aspects of the non-local measurements of Hubble constant in CMB and baryon acoustic oscillation (BAO) measurements are considered. In Chapter 5, meaning of the Hubble tension is discussed concisely and concretely. In Chapter 6, we study basic aspects of scalar field models proposed for solution of the Hubble tension by considering three models from late solutions and three models from early time solutions. Finally, in Chapter 7 we conclude.

CHAPTER 2

BRIEF OVERVIEW OF THE STANDARD MODEL OF COSMOLOGY

2.1. Background Evolution

2.1.1. Robertson-Walker Metric

Cosmological observations suggest that universe at scales larger than clusters of galaxies (at an instant of time) seem to be isotropic (when overaged over large scales)[58]. We assume that the universe seems to be isotropic at these scales when viewed from any point in the universe. These together imply that the universe is homogeneous and isotropic at any instant of time which is called cosmological principle. Moreover, we may assume this to be true at any time during the evolution of the universe by Weyl's postulate [58]. This, in turn, implies that the metric describing the universe (at cosmological scales) is described by Robertson-Walker (RW) metric, namely, [97]

$$ds^2 = g_{\mu\nu}dx^\mu dx^\nu = -dt^2 + a^2\left(\frac{dr^2}{1-kr^2} + r^2 d\Omega^2\right) \ , \quad \text{where} \quad d\Omega^2 \equiv d\theta^2 + \sin^2\theta d\phi^2 \tag{2.1}$$

where $a = a(t)$ is called scale factor, k specifies the three dimensional curvature, and $k = 1, 0, -1$ for closed, flat, open universes, respectively. The derivation of the RW metric is presented in Appendix A.

2.1.2. Friedmann-Lemaître-Robertson-Walker Universe

After substituting RW metric and the corresponding energy-momentum tensor in Einstein's field equations, we obtain a set of equations that are called Friedmann

equations. The resulting universe is called the Friedmann-Lemaître-Robertson-Walker (FLRW) universe.

First, we take a look at the general form of Einstein Equations:

$$R_{\mu\nu} - \frac{R}{2} g_{\mu\nu} - \Lambda g_{\mu\nu} = 8\pi G T_{\mu\nu} \tag{2.2}$$

where G is Newton's constant, $T_{\mu\nu}$ is the energy-momentum tensor, Λ is the cosmological constant, and $R_{\mu\nu}$ is Ricci tensor, R is the curvature scalar which is the contracted Ricci tensor, namely,

$$R_{\mu\nu} \equiv g^{\alpha\beta} R_{\alpha\mu\beta\nu} = R^{\beta}_{\ \mu\beta\nu} \ , \quad R \equiv g^{\mu\nu} R_{\mu\nu} \tag{2.3}$$

with $R^{\alpha}_{\ \delta\beta\gamma}$ being the Riemann-Christoffel tensor

$$R^{\alpha}_{\ \delta\beta\gamma} \equiv \Gamma^{\alpha}_{\ \delta\gamma,\beta} - \Gamma^{\alpha}_{\ \delta\beta,\gamma} - \Gamma^{\alpha}_{\ \epsilon\gamma}\Gamma^{\epsilon}_{\ \delta\beta} + \Gamma^{\alpha}_{\ \epsilon\beta}\Gamma^{\epsilon}_{\ \delta\gamma} \tag{2.4}$$

The homogeneity and isotropy of the universe may be described by a perfect fluid with the energy-momentum tensor

$$T_{\mu\nu} = (\rho + p)\, U_{\mu} U_{\nu} + p g_{\mu\nu} \tag{2.5}$$

where ρ is the energy density, p is the pressure, and U_{μ} is the four-velocity of the observer. At co-moving coordinates, where $(U_{\mu}) = (-1, 0, 0, 0)$, (2.5) reads

$$T_{\mu\nu} = \begin{pmatrix} \rho & 0 & 0 & 0 \\ 0 & p\,\frac{a^2(t)}{1-kr^2} & 0 & 0 \\ 0 & 0 & p\, a^2(t) r^2 & 0 \\ 0 & 0 & 0 & p\, a^2(t) r^2 \sin^2\theta \end{pmatrix} \tag{2.6}$$

By substituting the (2.1) and (2.6) in (2.2), one obtains the Friedmann equations:

$$H^2 \equiv \left(\frac{\dot{a}}{a}\right)^2 = \frac{8\pi G}{3}\rho - \frac{k}{a^2} \tag{2.7}$$

$$\frac{\ddot{a}}{a} = -\frac{4\pi G}{3}(\rho + 3p) \tag{2.8}$$

where H is the Hubble rate which is a measure of the expansion rate of the universe. We have also the continuity equation

$$\nabla_{\mu} T^{\mu 0} = \frac{\partial \rho}{\partial t} + 3\frac{\dot{a}}{a}(\rho + p) = \dot{\rho} + 3H(\rho + p) = 0 \tag{2.9}$$

which is the energy conservation equation. Note that, in this case i.e. in the case of Friedmann equations any two of (2.7), (2.8), and (2.9) equations are enough to describe the FLRW universe.

We may relate ρ and p by an equation of state (EoS) defined by

$$w = \frac{p}{\rho} \tag{2.10}$$

Equation (2.10) may be substituted in the continuity and Friedmann equations

$$\dot{\rho} + 3H(1+w)\rho = 0 \tag{2.11}$$

$$H^2 = \frac{8\pi G}{3}\rho - \frac{k}{a^2} \tag{2.12}$$

$$\frac{\ddot{a}}{a} = -\frac{4\pi G}{3}\rho(1+3w) \tag{2.13}$$

where any two of the resulting equations may be used to determine the corresponding universe explicitly.

2.2. Cosmological Perturbations

In the real universe at scales smaller than the scale of the clusters of galaxies, the grouping of matter appears as inhomogeneities in the universe. The degree of inhomogeneities at the scale of clusters of galaxies is initially small enough to call them perturbations. For instance, one of the most well-known cosmological perturbations is the temperature perturbation which can be expressed as

$$\delta T = T - \bar{T} \quad , \quad \delta_T = \frac{\delta T}{\bar{T}} \tag{2.14}$$

where $\bar{T}$ is the unperturbed temperature or the temperature in the Robertson-Walker spacetime. In general relativistic treatment of perturbations we make a gauge choice that associates the real space-time with the unperturbed space-time. Hence, we can use the well known FLRW universe to understand the behavior of the real universe. To understand the cosmological perturbations, let us consider a general background metric $\bar{g}_{\mu\nu}$. In general this metric may be perturbed as

$$g_{\mu\nu} = \bar{g}_{\mu\nu} + \delta g_{\mu\nu} = \bar{g}_{\mu\nu} + h_{\mu\nu} \tag{2.15}$$

One may express the metric component perturbations in the form

$$\begin{aligned} h_{00} &= -E \\ h_{i0} &= a\left[\partial_i F + G_i\right] \\ h_{ij} &= a^2\left[A\delta_{ij} + \partial_i\partial_j B + \partial_j C_i + \partial_i C_j + D_{ij}\right] \end{aligned} \tag{2.16}$$

This form helps performing scalar-vector- tensor decomposition of the perturbations. After the composition we get scalars (i.e.A, B, E, F), divergenceless vectors (i.e.$\partial_i C_i = \partial_i G_i = 0$), and divergenceless traceless symmetric tensors (i.e.$\partial_i D_{ij} = 0, D_{ii} = 0$) that are independent and uncoupled to each other. The explicit form of the perturbation of RW metric can be written as

$$\begin{aligned} ds^2 &= (\bar{g}_{\mu\nu} + h_{\mu\nu}) dx^\mu dx^\nu \\ &= -(1+E)dt^2 + a\left[\partial_i F + G_i\right] dt dx^i + a^2\left[(1+A)\delta_{ij} + \partial_i\partial_j B + \partial_j C_i + \partial_i C_j + D_{ij}\right] dx^i dx^j \end{aligned} \tag{2.17}$$

A metric ds^2 is invariant under a general coordinate transformation given by $x^\mu \to \hat{x}^\mu = x^\mu + \epsilon^\mu(x)$. One can write gauge transformations where only the field perturbations are affected by such a coordinate transformation so that $h_{\mu\nu}(x) \to h_{\mu\nu} + \Delta h_{\mu\nu}$ with

$$\Delta h_{\mu\nu}(x) \equiv \hat{g}_{\mu\nu}(x) - g_{\mu\nu}(x) \tag{2.18}$$

where $\Delta h_{\mu\nu}$ is an unphysical perturbation due to gauge transformation. This implies that some components of $g_{\mu\nu}$ are unphysical, so may be eliminated. In general $\hat{g}_{\mu\nu}$ denotes the form of $g_{\mu\nu}$ after the gauge transformation

$$\hat{g}_{\mu\nu}(x) = \bar{g}_{\mu\nu}(x) + h_{\mu\nu}(x) + \Delta h_{\mu\nu}(x) \tag{2.19}$$

One can write $\hat{g}_{\mu\nu}(\hat{x})$ by starting from the line element and applying the infinitesimal diffeomorphism i.e. $\hat{x}^\mu = x^\mu + \epsilon^\mu$ or similarly $x^\mu = \hat{x}^\mu - \epsilon^\mu$,

$$g_{\mu\nu}(x) dx^\mu dx^\nu = g_{\mu\nu}(\hat{x} - \epsilon) \frac{\partial x^\mu}{\partial \hat{x}^\lambda} \frac{\partial x^\nu}{\partial \hat{x}^\sigma} d\hat{x}^\lambda d\hat{x}^\sigma \tag{2.20}$$

as $dx^\mu = \frac{\partial x^\mu}{\partial \hat{x}^\lambda} d\hat{x}^\lambda = \left(\delta^\mu_\lambda - \frac{\partial \epsilon^\mu}{\partial \hat{x}^\lambda}\right) d\hat{x}^\lambda$. Hence

$$g_{\mu\nu}(x) dx^\mu dx^\nu = g_{\mu\nu}(\hat{x} - \epsilon) \left(\delta^\mu_\lambda - \frac{\partial \epsilon^\mu}{\partial \hat{x}^\lambda}\right) d\hat{x}^\lambda \left(\delta^\nu_\sigma - \frac{\partial \epsilon^\nu}{\partial \hat{x}^\sigma}\right) d\hat{x}^\sigma \tag{2.21}$$

$g_{\mu\nu}(\hat{x} - \epsilon)$ can be written to first order in ϵ^μ as

$$g_{\mu\nu}(\hat{x} - \epsilon) \simeq g_{\mu\nu}(\hat{x}) - \epsilon^\lambda \frac{\partial g_{\mu\nu}(\hat{x})}{\partial \hat{x}^\lambda} \tag{2.22}$$

So Eq. (2.21) becomes

$$\begin{aligned} g_{\mu\nu}(x) dx^\mu dx^\nu &= \left[g_{\mu\nu}(\hat{x}) - \epsilon^\lambda \frac{\partial g_{\mu\nu}(\hat{x})}{\partial \hat{x}^\lambda}\right] \left(\delta^\mu_\rho - \frac{\partial \epsilon^\mu}{\partial \hat{x}^\rho}\right) d\hat{x}^\rho \left(\delta^\nu_\sigma - \frac{\partial \epsilon^\nu}{\partial \hat{x}^\sigma}\right) d\hat{x}^\sigma \\ &= g_{\mu\nu}(\hat{x}) d\hat{x}^\mu d\hat{x}^\nu - g_{\mu\nu}(\hat{x}) \frac{\partial \epsilon^\mu}{\partial \hat{x}^\rho} d\hat{x}^\rho d\hat{x}^\nu - g_{\mu\nu}(\hat{x}) \frac{\partial \epsilon^\nu}{\partial \hat{x}^\sigma} d\hat{x}^\mu d\hat{x}^\sigma \\ &\quad - \epsilon^\lambda \frac{\partial g_{\mu\nu}(\hat{x})}{\partial \hat{x}^\lambda} d\hat{x}^\mu d\hat{x}^\nu \end{aligned} \tag{2.23}$$

i.e.

$$g_{\mu\nu}(x)dx^\mu dx^\nu = \left[g_{\mu\nu}(\hat{x}) - g_{\rho\nu}(\hat{x})\frac{\partial\epsilon^\rho}{\partial\hat{x}^\mu} - g_{\mu\sigma}(\hat{x})\frac{\partial\epsilon^\sigma}{\partial\hat{x}^\nu} - \epsilon^\lambda\,\frac{\partial g_{\mu\nu}(\hat{x})}{\partial\hat{x}^\lambda}\right] d\hat{x}^\mu d\hat{x}^\nu \tag{2.24}$$

$$= \hat{g}_{\mu\nu}(\hat{x})d\hat{x}^\mu d\hat{x}^\nu \tag{2.25}$$

where

$$\hat{g}_{\mu\nu}(\hat{x}) = g_{\mu\nu}(\hat{x}) - g_{\rho\nu}(\hat{x})\frac{\partial\epsilon^\rho}{\partial\hat{x}^\mu} - g_{\mu\sigma}(\hat{x})\frac{\partial\epsilon^\sigma}{\partial\hat{x}^\nu} - \epsilon^\lambda\,\frac{\partial g_{\mu\nu}(\hat{x})}{\partial\hat{x}^\lambda} \tag{2.26}$$

Hence,

$$\Delta h_{\mu\nu}(x) = \hat{g}_{\mu\nu}(x) - g_{\mu\nu}(x) = -g_{\mu\lambda}(x)\partial_\nu\epsilon^\lambda - g_{\lambda\nu}(x)\partial_\mu\epsilon^\lambda - \partial_\lambda g_{\mu\nu}(x)\epsilon^\lambda \tag{2.27}$$

Or explicitly

$$\begin{aligned}
\Delta h_{00} &= -2\partial_0\epsilon_0 \\
\Delta h_{i0} &= -\partial_0\epsilon_i - \partial_i\epsilon_0 + 2\frac{\dot{a}}{a}\epsilon_i \\
\Delta h_{ij} &= -\partial_j\epsilon_i - \partial_i\epsilon_j + 2a\dot{a}\delta_{ij}\epsilon_0
\end{aligned} \tag{2.28}$$

Decomposing the spatial component of ϵ^μ into the gradient of a spatial scalar and a divergenceless vector (i.e. $\partial_i\epsilon_i^V = 0$) is required:

$$\epsilon_i = \partial_i\epsilon^S + \epsilon_i^V \tag{2.29}$$

One may use (2.29) to write

$$\begin{aligned}
h_{00} + \Delta h_{00} &= -E - 2\partial_0\epsilon_0 \\
h_{i0} + \Delta h_{i0} &= a\left[\partial_i F + G_i\right] - \partial_0\partial_i\epsilon^S - \partial_0\epsilon_i^V - \partial_i\epsilon_0 + 2\frac{\dot{a}}{a}\partial_i\epsilon^S + 2\frac{\dot{a}}{a}\epsilon_i^V \\
h_{ij} + \Delta h_{ij} &= a^2\left[A\delta_{ij} + \partial_i\partial_j B + \partial_j C_i + \partial_i C_j + D_{ij}\right] - \partial_j\partial_i\epsilon^S \\
&\quad - \partial_j\epsilon_i^V - \partial_i\partial_j\epsilon^S - \partial_i\epsilon_j^V + 2a\dot{a}\delta_{ij}\epsilon_0
\end{aligned} \tag{2.30}$$

Now, to get rid of the unphysical scalars we need to determine the physical parameters by fixing the gauge. Considering the scalar modes, the perturbed metric becomes

$$\begin{aligned}
ds^2 = &-(1 + E + 2\partial_0\epsilon_0)dt^2 + \partial_i\left(a\,F - \partial_0\epsilon^S - \epsilon_0 + 2\frac{\dot{a}}{a}\epsilon^S\right)dtdx^i \\
&+ \left(a^2\left[1 + A + 2\frac{\dot{a}}{a}\epsilon_0\right]\delta_{ij} + \partial_i\partial_j\left[a^2B - 2\epsilon^S\right]\right)dx^i dx^j
\end{aligned} \tag{2.31}$$

We choose Newtonian gauge, adjust ϵ^S in order to get $B' = \partial_i\partial_j\left[a^2B - 2\epsilon^S\right] = 0$, and ϵ_0 so that $F' = \partial_i\left(a\,F - \partial_0\epsilon^S - \epsilon_0 + 2\frac{\dot{a}}{a}\epsilon^S\right) = 0$. In this gauge, it's conventional to use $E' = E + 2\partial_0\epsilon_0$ and $A' = A + 2\frac{\dot{a}}{a}\epsilon_0$ as

$$E' \equiv 2\Phi\ , \quad A' \equiv -2\Psi \tag{2.32}$$

without less of generality we may express the perturbed metric as

$$ds^2 = -(1+2\Phi)dt^2 + a^2\delta_{ij}(1-2\Psi)dx^i dx^j \tag{2.33}$$

here Φ is the gravitational potential, Ψ is scale factor average local perturbation.

The Einstein field equations for the expansion of the unperturbed case can be expressed as

$$\bar{R}_{\mu\nu} = 8\pi G\bar{S}_{\mu\nu} \tag{2.34}$$

its perturbation is

$$\delta R_{\mu\nu} = 8\pi G\delta S_{\mu\nu} \tag{2.35}$$

where $S_{\mu\nu}$ is the source tensor that can be expressed as

$$S_{\mu\nu} = T_{\mu\nu} - \frac{1}{2}g_{\mu\nu}g^{\rho\sigma}T_{\rho\sigma} \tag{2.36}$$

First, one must use the perturbed affine connection to find the perturbed Ricci tensor as [9, 97]:

$$\delta R_{\mu\kappa} = \frac{\partial\,\delta\Gamma^{\lambda}_{\mu\lambda}}{\partial x^{\kappa}} - \frac{\partial\,\delta\Gamma^{\lambda}_{\mu\kappa}}{\partial x^{\lambda}} + \delta\Gamma^{\eta}_{\mu\nu}\bar{\Gamma}^{\nu}_{\kappa\eta} + \delta\Gamma^{\nu}_{\kappa\eta}\bar{\Gamma}^{\eta}_{\mu\nu} - \delta\Gamma^{\eta}_{\mu\kappa}\bar{\Gamma}^{\nu}_{\nu\eta} - \delta\Gamma^{\nu}_{\nu\eta}\bar{\Gamma}^{\eta}_{\mu\kappa} \tag{2.37}$$

and the perturbed energy-momentum tensor to find the perturbed source tensor $\delta S_{\mu\nu}$:

$$\delta S_{\mu\nu} = \delta T_{\mu\nu} - \frac{1}{2}\bar{g}_{\mu\nu}\delta T^{\lambda}_{\lambda} - \frac{1}{2}h_{\mu\nu}\bar{T}^{\lambda}_{\lambda} \tag{2.38}$$

Recall that the unperturbed energy-momentum tensor takes the form of the perfect fluid as we have shown in Eq. (2.5). Here

$$\bar{T}_{\mu\nu} = (\bar{\rho}+\bar{p})\,\bar{U}_{\mu}\bar{U}_{\nu} + \bar{p}\bar{g}_{\mu\nu} \tag{2.39}$$

and

$$\delta T^{\mu}_{\nu} = \bar{g}^{\mu\nu}\left[\delta T_{\lambda\nu} - h_{\lambda\kappa}\bar{T}^{\kappa}_{\nu}\right] \tag{2.40}$$

Thus, the perturbed Einstein equations read [97]:

$$4\pi Ga^2[\delta\rho - \delta p - \nabla^2\pi^2] = a\dot{a}\dot{\Phi} + 4\dot{a}^2\Phi + 2a\ddot{a}\Phi - \nabla^2\Psi + a^2\ddot{\Psi} + 6a\dot{a}\dot{\Psi} \tag{2.41}$$

$$-8\pi Ga(\bar{\rho}+\bar{p})\partial_j\delta u = -2\dot{a}\partial_j\Phi - 2a\partial_j\dot{Psi} \tag{2.42}$$

$$4\pi G[\delta\rho + 3\delta p + \nabla^2\pi^S] = -\frac{1}{a}\left[\frac{1}{a}\nabla^2\Phi + 3\dot{a}\dot{\Phi} + 3\ddot{Psi} + 6\dot{a}\dot{\Psi} + 6\ddot{a}\Phi\right] \tag{2.43}$$

2.3. Baryon-Photon Fluid Before Decoupling

The main aim of this section is to derive the equation for the baryon-photon wave and show that this wave has sound speed c_s. We start by writing an equation to describe how particles move from one phase-space point to another as

$$\frac{df}{dt} = C[f] \tag{2.44}$$

where f is called distribution function (i.e. occupation number) and it represents the number density in phase space (i.e. the number of particles per volume per momentum volume), and $C[f]$ is the source term (i.e. the collision term). $C[f] = 0$ corresponds to free particles and follows from conservation of the number density in phase space in the absence of external forces. The number of particles is conserved with a given momentum in co-moving coordinates if any particle-particle interactions are neglected. But when particle-particle interactions are considered, the source term should be included. The total derivative on the left hand side can be written using the partial derivatives in the form

$$\frac{df(\boldsymbol{x}, p, \hat{\boldsymbol{p}}, t)}{dt} = \frac{\partial f}{\partial t} + \frac{\partial f}{\partial x^i} \cdot \frac{dx^i}{dt} + \frac{\partial f}{\partial p}\frac{dp}{dt} + \frac{\partial f}{\partial \hat{p}^i} \cdot \frac{d\hat{p}^i}{dt} \tag{2.45}$$

One may use the geodesic equations for photons so we can express [30]

$$\frac{dx^i}{dt} = \frac{\hat{p}^i}{a}(1 + \Psi - \Phi) \tag{2.46}$$

and

$$\frac{1}{p}\frac{dp}{dt} = -H - \frac{\partial \Phi}{\partial t} - \frac{\hat{p}^i}{a}\frac{\partial \Psi}{\partial x^i} \tag{2.47}$$

One can substitute (2.46) and (2.47) in (2.45) with neglecting the last term and any other second order term to write the Boltzmann equation for photons as

$$\frac{df}{dt} = \frac{\partial f}{\partial t} + \frac{\hat{p}^i}{a}\frac{\partial f}{\partial x^i} - p\frac{\partial f}{\partial p}\left[H + \frac{\partial \Phi}{\partial t} + \frac{\hat{p}^i}{a}\frac{\partial \Psi}{\partial x^i}\right] \tag{2.48}$$

Now, let us take Bose-Einstein of the distribution function of photons, f in the presence of a temperature perturbation Θ

$$f(\boldsymbol{x}, p, \hat{\boldsymbol{p}}, t) = \left[e^{\frac{p}{T(t)[1+\Theta(\boldsymbol{x}, \hat{\boldsymbol{p}}, t)]}} - 1\right]^{-1} \simeq f^{(0)} - p\frac{\partial f^{(0)}}{\partial p}\Theta \tag{2.49}$$

where $f^{(0)} \equiv [e^{\frac{p}{T}} - 1]^{-1}$, T is the temperature which is a function only of time and it does not depend on $\boldsymbol{x}$ nor on the direction of propagation $\hat{p}$. But Θ depends on $\boldsymbol{x}$ and $\hat{p}$ because of the inhomogeneities and the anisotropies in the photon distribution. While it does not depend on the magnitude of the momentum p.

We may now go ahead and gather the terms in Eq. (2.48) that are comparable in order after substituting (2.49) in it. We can get benefit from the zeroth order [30] to get the relation between the temperature and the scale factor as $\frac{dT}{T} = -\frac{da}{a}$. We are interested in the first order term

$$\left.\frac{df}{dt}\right|_{\text{first order}} = -p\frac{\partial}{\partial t}\left[\frac{\partial f^{(0)}}{\partial p}\Theta\right] - p\frac{\hat{p}^i}{a}\frac{\partial\Theta}{\partial x^i}\frac{\partial f^{(0)}}{\partial p} + H\Theta p\frac{\partial}{\partial p}\left[p\frac{\partial f^{(0)}}{\partial p}\right] - p\frac{\partial f^{(0)}}{\partial p}\left[\frac{\partial\Phi}{\partial t} + \frac{\hat{p}^i}{a}\frac{\partial\Psi}{\partial x^i}\right] \tag{2.50}$$

using $\frac{\partial f^{(0)}}{\partial t} = -\frac{dT/dt}{T}p\frac{\partial f^{(0)}}{\partial p}$ where we have used $p \propto T \propto \frac{1}{a}$, the first order can be written as

$$\left.\frac{df}{dt}\right|_{\text{first order}} = -p\frac{\partial f^{(0)}}{\partial p}\left[\frac{\partial\Theta}{\partial t} + \frac{\hat{p}^i}{a}\frac{\partial\Theta}{\partial x^i} + \frac{\partial\Phi}{\partial t} + \frac{\hat{p}^i}{a}\frac{\partial\Psi}{\partial x^i}\right] \tag{2.51}$$

The first two terms explain how the distribution function changes when there are no collisions. The gravitational impact of perturbations is taken into consideration in the last two. We know that there will be a nonzero collision term at first order in perturbations, therefore this equation for Θ is not complete.

Next, We can consider the right side of Eq. (2.44). The general form of collision term is [30]

$$\begin{aligned} C[f_1(\boldsymbol{p})] = \frac{1}{2E_1(p)}\int\frac{d^3q}{(2\pi)^3 2E_2(q)}\int\frac{d^3p'}{(2\pi)^3 2E_3(p')}\int\frac{d^3q'}{(2\pi)^3 2E_4(q')}|\mathcal{M}|^2 \\ \times (2\pi)^4\delta_D^{(3)}[\boldsymbol{p}+\boldsymbol{q}-\boldsymbol{p}'-\boldsymbol{q}']\delta_D^{(1)}[E_1(p)+E_2(q)-E_3(p')-E_4(q')] \\ \times\{f_3(\boldsymbol{p}')f_4(\boldsymbol{q}')[1\pm f_1(\boldsymbol{p})][1\pm f_2(\boldsymbol{q})] \\ -f_1(\boldsymbol{p})f_2(\boldsymbol{q})[1\pm f_3(\boldsymbol{p}')][1\pm f_4(\boldsymbol{q}')]\} \end{aligned} \tag{2.52}$$

where energy and momentum conservations are enforced by the Dirac delta functions. Here, the microphysical characteristics of the interaction determine the scattering amplitude squared $|\mathcal{M}|^2$. Let us consider Compton scattering $e^-(\boldsymbol{q}) + \gamma(\boldsymbol{p}) \leftrightarrow e^-(\boldsymbol{q}') + \gamma(\boldsymbol{p}')$. The corresponding collision term is

$$\begin{aligned} C[f(\boldsymbol{p})] = \frac{1}{2E(p)}\int\frac{d^3q}{(2\pi)^3 2E_e(q)}\int\frac{d^3q'}{(2\pi)^3 2E_e(q')}\int\frac{d^3p'}{(2\pi)^3 2E(p')}\sum_{\text{3spins}}|\mathcal{M}|^2 \\ \times (2\pi)^4\delta_D^{(3)}[\boldsymbol{p}+\boldsymbol{q}-\boldsymbol{p}'-\boldsymbol{q}']\delta_D^{(1)}[E(p)+E_e(q)-E(p')-E_e(q')] \\ \times\{f_e(\boldsymbol{p}')f(\boldsymbol{q}') - f_e(\boldsymbol{q})f(\boldsymbol{p})\} \end{aligned} \tag{2.53}$$

where the photon energies are $E(p) = p$ and $E(p') = p'$. However, for electrons, we take the nonrelativistic limit and take it approximately be m_e. After we do the q' integration

and using the three-dimensional momentum delta function, we obtain

$$C[f(\boldsymbol{p})] = \frac{\pi}{2m_e p}\int \frac{d^3q}{(2\pi)^3 2m_e}\int \frac{d^3p'}{(2\pi)^3 2p'}\delta_D^{(1)}[p + E_e(q) - p' - E_e(|\boldsymbol{q}+\boldsymbol{p}-\boldsymbol{p'}|)] \times \sum_{3\text{ spins}} |\mathcal{M}|^2\{f_e(\boldsymbol{q}+\boldsymbol{p}-\boldsymbol{p'})f(\boldsymbol{p'}) - f_e(\boldsymbol{q})f(\boldsymbol{p})\} \tag{2.54}$$

using $E_e(q) - E_e(|\boldsymbol{q}+\boldsymbol{p}-\boldsymbol{p'}|) \simeq \frac{(\boldsymbol{p'}-\boldsymbol{p})\cdot\boldsymbol{q}}{m_e}$ and $f_e(\boldsymbol{q}+\boldsymbol{p}-\boldsymbol{p'}) \simeq f(\boldsymbol{q})$, one approximately can write

$$C[f(\boldsymbol{p})] = \frac{\pi}{2m_e p}\int \frac{d^3q}{(2\pi)^3 2m_e} f_e(\boldsymbol{q})\int \frac{d^3p'}{(2\pi)^3 2p'}\sum_{3\text{ spins}} |\mathcal{M}|^2 \times \left\{\delta_D^{(1)}(p-p') + \frac{(\boldsymbol{p'}-\boldsymbol{p})\cdot\boldsymbol{q}}{m_e}\frac{\partial}{\partial p'}\delta_D^{(1)}(p-p')\right\}\{f(\boldsymbol{p'}) - f(\boldsymbol{p})\} \tag{2.55}$$

The CMB found to exhibit a polarization due to the polarization dependency of the amplitude for Compton scattering. However, since the influence of polarization is negligible in the determination of the collision term, we will disregard it on radiation field. Additionally, we will also neglect the angular dependence changes due to its subdominant contribution to the collision term. Hence after these assumptions, for our case of the Compton scattering the amplitude squared is $\sum_{3\text{spins}} |\mathcal{M}|^2 = 32\pi\sigma_T m_e^2$, where σ_T is the Thomson cross-section [30]. Moreover, for the terms that are independent of $\boldsymbol{q}$, the q integral yields a factor of $n_e/2$ (the number 2 represents an electron's two possible spin states, which is denoted by $g_e = 2$). Conversely, terms with a factor of $\boldsymbol{q}/m_e$ produce $n_e\boldsymbol{u}_b/2$, where $\boldsymbol{u}_b$ is the bulk electron velocity. With these, and after substituting (2.49) in (2.55), the collision term becomes

$$C[f(\boldsymbol{p})] = -p\frac{\partial f^{(0)}}{\partial p} n_e\sigma_T[\Theta_0 - \Theta(\hat{\boldsymbol{p}}) + \hat{\boldsymbol{p}}\cdot\boldsymbol{u}_{\rm b}] \tag{2.56}$$

where Θ_0 is temperature monopole which is the integral of Θ over all directions of temperature. Now, substitute (2.51) and (2.56) in (2.44) to get the Boltzmann equation for photons, and simplify it cancelling similar factors and using the conformal time

$$\frac{\partial\Theta}{\partial\eta} + \hat{p}^i\frac{\partial\Theta}{\partial x^i} + \frac{\partial\Phi}{\partial\eta} + \hat{p}^i\frac{\partial\Psi}{\partial x^i} = n_e\sigma_T a[\Theta_0 - \Theta(\hat{\boldsymbol{p}}) + \hat{\boldsymbol{p}}\cdot\boldsymbol{u}_{\rm b}] \tag{2.57}$$

It is useful to write it in the momentum space (express it by tilde e.g. $\tilde{\Theta}(\boldsymbol{k})$) using Fourier transformation and defining the optical depth τ, and μ which is the cosine of the angle formed by the photon direction $\hat{p}$ and wavenumber $\boldsymbol{k}$. Hence,

$$\frac{\partial\tilde{\Theta}}{\partial\eta} + ik\mu\tilde{\Theta} + \frac{\partial\tilde{\Phi}}{\partial\eta} + ik\mu\tilde{\Psi} = -\frac{d\tau}{d\eta}[\tilde{\Theta}_0 - \tilde{\Theta} + \mu u_{\rm b}] \tag{2.58}$$

The Boltzmann equation for photons (2.48) is actually a special case of more general form for baryons where instead of using $E = p$, we have

$$\frac{df_{\rm b}}{dt} = \frac{\partial f_{\rm b}}{\partial t} + \frac{p}{E}\frac{\hat{p}^i}{a}\frac{\partial f_{\rm b}}{\partial x^i} - p\frac{\partial f_{\rm b}}{\partial p}\left[H + \frac{\partial \Phi}{\partial t} + \hat{p}^i\frac{E}{ap}\frac{\partial \Psi}{\partial x^i}\right] = C[f_{\rm b}] \tag{2.59}$$

The cosmic generalization of the continuity equation and the Euler equation for the baryon are obtained by using the zeroth and the first moment of the Boltzmann equations respectively. Integrate them after multiplying both sides by the phase space volume $\frac{d^3p}{(2\pi)^3}$ and using the definitions of the fluid velocity $u^i_{\rm b} = \frac{1}{n_{\rm b}}\int \frac{d^3p}{(2\pi)^3} f_{\rm b}\frac{p\hat{p^i}}{E}$ and the density of baryons $n_{\rm b} = \int \frac{d^3p}{(2\pi)^3} f_{\rm b}$. Subsequently, using the first-order equations in Fourier space and conformal time, we get [30]

$$\frac{d\delta'_{\rm b}}{d\eta} + iku_{\rm b} = -3\frac{d\Phi}{d\eta} \tag{2.60}$$

$$\frac{u_{\rm b}}{d\eta} + \frac{a'}{a}u_{\rm b} = -ik\Psi + \frac{1}{R}\frac{d\tau}{d\eta}[u_{\rm b} + 3i\Theta_1], \text{ or equivalently}$$

$$u_{\rm b} = -3i\Theta_1 + \frac{R}{\frac{d\tau}{d\eta}}\left[\frac{du_{\rm b}}{d\eta} + \frac{a'}{a}u_{\rm b} + ik\Psi\right] \tag{2.61}$$

where R is the baryon-to-photon energy ratio $R \equiv \frac{3\rho_b}{4\rho_\gamma}$. By using the definition of the lth temperature multipole moment Θ_l

$$\Theta_l(k,\eta) \equiv \frac{1}{(-i)^l}\int_{-1}^{1}\frac{d\mu}{2}\mathcal{P}_l(\mu)\Theta(\mu,k,\eta) \tag{2.62}$$

where $\mu \equiv \frac{\boldsymbol{k}\cdot\hat{\boldsymbol{p}}}{k}$, and η is the conformal time. One can use the completeness of the Legendre function to write

$$\Theta(\mu,k,\eta) = \sum_{l=0}^{\infty} A_l\mathcal{P}_l(\mu)\ , \quad \text{where} \quad A_l(k,\eta) = \frac{2l+1}{2}\int_{-1}^{1}\Theta(\mu,k,\eta)\mathcal{P}_l(\mu) \tag{2.63}$$

Hence, using (2.62) we equivalently write

$$\Theta(\mu,k,\eta) = \sum_{l=0}^{\infty}(2l+1)(-i)^l\Theta_l(k,\eta)\mathcal{P}_l(\mu) \tag{2.64}$$

We can integrate over μ after multiplying (2.58) by $\mathcal{P}_0(\mu) = 1$ and $\mathcal{P}_1(\mu) = \mu$ respectively

$$\frac{\partial\Theta_0}{\partial\eta} + k\Theta_1 = \frac{\partial\Phi}{\partial\eta}, \text{ or equivalently} \qquad k\Theta_1 = \frac{\partial\Phi}{\partial\eta} - \frac{\partial\Theta_0}{\partial\eta} \tag{2.65}$$

$$\frac{\partial\Theta_1}{\partial\eta} - \frac{k\Theta_0}{3} = \frac{k\Psi}{3} + \frac{d\tau}{d\eta}[\Theta_1 - \frac{iu_{\rm b}}{3}] \tag{2.66}$$

One can approximate (2.61) to the lowest order as $u_{\rm b} = -3i\Theta_1$ to rewrite the bracket in (2.61) as

$$u_{\rm b} \simeq -3i\Theta_1 + \frac{R}{\frac{d\tau}{d\eta}}\left[-3i\frac{d\Theta_1}{d\eta} - 3i\frac{a'}{a}\Theta_1 + ik\Psi\right] \tag{2.67}$$

Hence, one can substitute it in (2.66)

$$\frac{\partial \Theta_1}{\partial \eta} + \frac{a'}{a}\frac{R}{1+R}\Theta_1 - \frac{k}{3(1+R)}\Theta_0 = \frac{k\Psi}{3} \tag{2.68}$$

substituting (2.65) in this equation gives us a second order wave equation

$$\frac{\partial^2 \Theta_0}{\partial \eta^2} + \frac{a'}{a}\frac{R}{1+R}\frac{\partial \Theta_0}{\partial \eta} + k^2 c_s^2 \Theta_0 = -\frac{k^2}{3}\Psi - \frac{a'}{a}\frac{R}{1+R}\frac{\partial \Phi}{\partial \eta} - \frac{\partial^2 \Phi}{\partial \eta^2} \tag{2.69}$$

where c_s is the sound speed of the baryon-photon wave

$$c_s(\eta) \equiv \sqrt{\frac{1}{3(1+R[\eta])}} \tag{2.70}$$

In other words, it is shown that the photon-baryon fluid before decoupling moves as a wave (with a damping and driving force term) with velocity c_s given in (2.70).

CHAPTER 3

COSMIC DISTANCE LADDER AND LOCAL MEASUREMENTS OF HUBBLE CONSTANT

3.1. Cosmic Distance Ladder

The cosmic distances where Hubble flow is the main source of redshift of light coming from celestial objects may be determined by using a sequence of measurements that is called the cosmic distance ladder. The first rung of the ladder is the measurement of the distances of nearby objects where the effect of Hubble expansion on the motion of the astronomical objects is wholly negligible. The methods used for these relatively small distances are called primary distance indicators. In this context, the distances of the most nearby stars may be determined by the geometrical parallax method and other primary distance indicators such as main sequence stars. The minimum distances that may be measured by main sequence stars are in the order of the largest distances that can be measured by trigonometric parallax. Hence trigonometric parallax may be used to calibrate the main sequence method. For example, [88] employs the main sequence fitting method to determine the distance of the globular galactic cluster NGC5904 (M5) whose distance had been also determined by the geometric parallax method [67]. Similar procedures may be used for other primary distance indicators. This enables measuring further distances and cross-checking between different methods.

The second step of distance measurements are called secondary distance indicators. These are mainly the methods that can measure the effect of Hubble expansion, so are able to measure H_0 while they cannot be used to determine if the expansion of the universe is accelerating or not. They correspond to distances roughly in the interval of $0.03 \lesssim z \lesssim 0.1$.

The final step of the cosmic ladder expansion is mainly supernovae. There are supernovae that are close enough so that they may be calibrated by secondary distance indicators. e.g. cepheids. In fact, cepheids have a very unique position in this aspect. Some cepheids are close enough so that their distances may be calibrated by primary distance indicators while there are cepheids that are far enough so that can be used to

calibrate supernovae distances.

3.2. Main Measurement Methods for Very Low Redshift Distances: Primary Distance Indicators

The objects used to measure distances in cosmology are divided into primary and secondary distance indicators. In this section, we will consider the main methods to determine low redshift distances(z not much greater than 0.01) [97]. Here we will consider the primary distance indicators. The two main classic kinematic methods are used to determine the distance of objects within our own galaxy($z \lesssim 0.01$) [97]. They are important in determining almost all distance measurements in astronomy.

3.2.1. Trigonometric Parallax

Trigonometric parallax is an essential tool in determining the distances to nearby stars. To understand it, let's consider the motion of Earth around the Sun. As Earth orbits the Sun, nearby stars appear to shift their positions slightly relative to more distant stars. This apparent shift is caused by the change in the observer's (in this case, the Earth's) position as it moves along its orbit. The angle of this apparent shift is called the parallax angle or trigonometric parallax π. It is the angle subtended at the star by the baseline formed by Earth's orbit around the Sun. The parallax angle can be measured by observing the apparent change in the star's position against the background of more distant stars over a period of six months, as the Earth moves from one side of its orbit to the other. So what we actually observe is twice the parallax angle 2π.

Using basic trigonometry, the distance to the star can be calculated from its parallax angle. This may be measured in terms of angle in radians by

$$\pi = \frac{d_E}{d} \tag{3.1}$$

where d_E is the mean distance of the earth from the sun, and d is the distance of the star from the sun. The parallax angle is typically very small, measured in arcseconds (1/3,600th of a degree). The parallax in seconds of arc is the reciprocal of the distance in parsecs. where a parsec (pc) is defined as the distance at which $\pi = 1''$.

3.2.2. Proper Motions and Apparent Luminosity

Proper motion (μ) refers to the apparent motion of a celestial object across the sky at a rate in radians/time, that is given by

$$\mu = \frac{v_\perp}{d} \tag{3.2}$$

where $v_\perp$ is the celestial object's velocity in the transverse direction to the line of sight, and d is the distance between the object and the earth. We may determine the component of velocity along the line of sight by analyzing the Doppler shift in the spectral lines of the source. Subsequently, we may compute $v_\perp$ by assuming that the velocities in the direction perpendicular to the line of sight are the same as the velocities along the line of sight, by spherical symmetry of the orbit of the observed object.

These kinematic techniques have limited use beyond our solar system. Greater distances necessitate alternative measurement approaches. In cosmology, the most prevalent technique for measuring distance involves measuring the apparent luminosity of objects with known absolute luminosities. The apparent luminosity ℓ is the energy received per second per square centimeter of the receiving area, whereas the absolute luminosity L is the energy released per second. The connection between absolute and apparent luminosity, as per Euclidean geometry, is as follows:

$$\ell = \frac{L}{4\pi d^2} \tag{3.3}$$

d is the distance between the object and the earth. By directly measuring ℓ and using L that is determined by another method, one may use the above formula to find d.

3.2.3. Some primary distance indicators to determine absolute luminosity

While two stars are never completely the same in the actual Universe, there are stellar objects with almost constant absolute luminosities regardless of their location in the sky. These are known as standard candles. Those and several different types of stars have been utilized in the observation of absolute luminosity that is needed to do the measurements of distance through. Here we give some examples of primary distance indicators:

3.2.3.1. Main Sequence

Main sequence stars are characterized as those that continue to burn hydrogen at their cores and exhibit a distinctive relation between absolute luminosity and color, both of which rely on mass. The highest luminosity is found in blue-white stars, diminishing gradually for hues that go toward yellow and red. Calibration of absolute luminosities of the main sequence involves stars with known distances, determined through trigonometric parallax measurements and apparent luminosity assessments. These distances, determined through this method, are occasionally referred to as photometric parallaxes [97].

3.2.3.2. Red Clump Stars

Red Clump Stars are a specific type of stars in the later stages of their evolution where have exhausted all of their hydrogen and burn helium instead. The absolute luminosity of Red Clump Stars is relatively well-defined especially in the infrared band, making them useful for distance estimation [97].

3.2.3.3. RR Lyrae Stars

RR Lyrae stars are low-mass variable stars whose luminosities fluctuate. By using statistical and trigonometric parallax methods their absolute luminosities are calibrated, and these calibrations are used to find their approximate absolute luminosities. After estimating their intrinsic luminosities, they can be used as distance indicators [97].

3.2.3.4. Eclipsing Binaries

Eclipsing binaries are systems consisting of a primary star and a smaller companion, where the smaller star periodically eclipses the primary star. The companion's velocity may be deduced from the Doppler shift of its spectral lines. The duration of the eclipse allows for the determination of the radius of the primary star, which in turn enables the calculation of its surface area. The temperature of the primary is found from the measurement of its spectrum. The absolute luminosity of the primary can then be calculated

using the Stefan-Boltzmann law of black body radiation [97]. Among the three types of eclipsing binary systems, the detached eclipsing binary systems (DEBs) are considered the most effective for determining distances. This serves as a solid anchor for the Magellanic Clouds as it provides the most precise distances known for the Large Magellanic Cloud (LMC) [69] and Small Magellanic Cloud (SMC) [39].

3.2.3.5. Masers

Water masers seen in the accretion disks of supermassive black holes (SMBHs) in active galactic nuclei (AGNs) offer a unique method for measuring geometric distances to their host galaxies. Very long baseline interferometric (VLBI) observations of the Masers' locations, velocities, and accelerations can reveal their Keplerian motion (as predicted for orbits around a point mass). This data may be utilized to get a purely geometric distance to the maser host galaxies. However, these objects are uncommon due to the necessity of an edge-on alignment of the inner accretion disk with our line of sight, along with an appropriate density profile of the disk [68, 74].

3.2.3.6. Cepheid Variables

Cepheid variables are stars whose luminosity is known to vary periodically. These are very bright stars that can be observed even outside their galaxies. They are used to measure the distances outside our galaxy. Leavitt showed in [52] that there is a tight relation between their period of pulsation (weeks to months) and their maximum detected flux. The Period-Luminosity Relation for Cepheid variables is typically given as:

$$M = a \log P + b \tag{3.4}$$

where M represents the absolute magnitude or intrinsic luminosity of the Cepheid variable, P represents the period (in days) of the Cepheid variable's pulsation, The slope of the line (coefficient "a" in the equation) determines the relationship between period and luminosity, while the intercept (coefficient "b") accounted for the absolute magnitude offset, and they depend on the specific wavelength or filter used for observations. One can convert period measurements of distant cepheids into absolute luminosity measurements by using Leavitt's law, providing us with the absolute distance to these variable stars.

3.2.3.7. Tip of the Red Giant Branch(TRGB)

The TRGB is the highest brightness point for red giant branch (RGB) stars, which are main-sequence stars. As an RGB star exhausts the hydrogen in its core producing helium, it transitions to burning hydrogen in a shell surrounding the core, gradually increasing the mass of the helium core. This leads to the star cooling down while becoming brighter, a progression that persists until the helium core's mass, and subsequently its temperature, reaches a sufficient level (approximately 0.5 solar masses) to trigger helium burning, transitioning to carbon. This event, akin to the sudden onset of helium fusion in low-mass stars, is known as the helium flash [47].

The TRGB is not a specific star, but rather a characteristic of a stellar distribution. Therefore, it is not as straightforward to determine its luminosity from trigonometric parallaxes as it is for individual stars such as Cepheid variables. To calibrate TRGB luminosity, it was essential to measure the distance to a group of stars that are at the same distance from us [35, 87].

3.3. Secondary Distance Indicators

The secondary distance indicators are calibration methods to measure the distances that are at redshifts sufficiently large for peculiar velocities (velocities of stars in the galaxy relative to the galaxy) to be insignificant compared to the expansion velocity (approximately $0.1 > z > 0.03$) [97].

3.3.1. Some secondary distance indicators to determine absolute luminosity

Here we give some examples of secondary distance indicators:

3.3.1.1. Tully-Fisher Relation

In 1977, Tully and Fisher [90] developed a method to estimate the absolute luminosity of suitable spiral galaxies. They utilized the 21 cm absorption line observed in

these galaxies, which arises from transitions of hydrogen atoms between their two hyperfine states. The Doppler effect, resulting from the rotation of the galaxy, causes the broadening of this absorption line (known as the Doppler shift of its spectral lines). The width of the line, denoted as W, provides an indication of the maximum rotational speed of the galaxy. This rotational speed is correlated with the galaxy's mass, which, in turn, is correlated with its absolute luminosity [1]. Therefore, by measuring the width of the hyperfine splitting lines, one can determine the rotational speed of the galaxy and, consequently, its absolute luminosity.

3.3.1.2. Faber-Jackson Relation

This method uses the relation between random velocities of stars in elliptical galaxies with their absolute luminosity to find the absolute luminosities of elliptical galaxies[33].

3.3.1.3. Fundamental Plane

This method is the improvement of the Faber-Jackson relation where the effect of the surface brightness of star clusters on the absolute luminosities is also taken into account[31].

3.3.2. Type Ia Supernovae

In the context of secondary distance indicators, it is essential to dedicate a separate subsection to consider type Ia supernovae emphasizing their profound significance.

Type Ia supernovae are thought to happen when a white dwarf star in a binary system gathers enough material from its companion to amplify its mass near the Chandrasekhar limit (the maximum mass supported by electron degeneracy pressure, which is an effective pressure that prevents white dwarfs from undergoing gravitational collapse). When the white dwarf exceeds this limit, it becomes unstable. The subsequent increase in temperature and density allows the conversion of carbon and oxygen into nickel, leading to a catastrophic collapse and thermonuclear explosion. The implication of this is that since such supernovae all start at about the same mass (i.e. the Chandrasekhar limit), their absolute luminosity ought to be constant for all such supernovae and therefore they pro-

vide high brightness "perfect standard candles" for distance measurement. Their absolute luminosity also depends on the declining time of supernova light, where the slower the decline, the higher the absolute luminosity.

In order to determine the absolute luminosity of Type Ia supernovae, since none of them are sufficiently close for a parallax measurement in the 400 years, some kind of calibration is required. These supernovae are significantly more luminous than primary distance indicators, with luminosities reaching billions of solar luminosities. One way to calibrate them is by using the cepheids. However, given that neighboring galaxies that host type Ia supernovae and cepheids are uncommon, an alternative set of calibrator galaxies can be obtained through the tip of the red giant branch (TRGB) method. The relation of absolute luminosity and decline time was calibrated using some supernovae in galaxies whose distance had been determined via the detection of cepheid variables they contained. The distances to a larger sample of additional type Ia supernovae in farther-off galaxies were subsequently computed using this relation.

3.4. Luminosity Distance

In subsection 3.2.2, we developed the common relation for the apparent brightness ℓ of a source with absolute luminosity L at a distance d. For distances at greater redshifts, say $z > 0.1$ [97], the effects of cosmic expansion on the measurement of distance cannot be ignored. Subsequently, the adjusted formula for a source's apparent brightness at radial coordinate r_1 at any redshift z is

$$\ell = \frac{L}{4\pi r_1^2 a(t_0)^2 (1+z)^2} \tag{3.5}$$

where $a(t_0)$ is the Robertson-Walker scale factor at the present time. This formula can be expressed as the previous one, by defining the luminosity distance d_L:

$$\ell = \frac{L}{4\pi d_L^2} \quad \text{where} \quad d_L = r_1 a(t_0)(1+z) \tag{3.6}$$

For nearby sources (objects with $z \ll 1$) [97], we can express the relation between luminosity distance and redshift effectively using a power series. This allows us to derive a representation of the luminosity distance (d_L) that explicitly shows its relation with the Hubble constant. It is useful to begin with the definition of the Hubble constant:

$$H_0(t) \equiv \frac{\dot{a}(t_0)}{a(t_0)} \tag{3.7}$$

H_0 can be used in expanding the Robertson-Walker scale factor a(t) in a power series, so

$$a(t) \approx a(t_0)[1 + (t - t_0)H_0 - \frac{1}{2}(t - t_0)^2(q_0 H_0^2) + \cdots] \tag{3.8}$$

Then the redshift can be expressed using the Hubble constant and the look-back time $(t_0 - t)$ as:

$$z = \frac{a(t_0)}{a(t)} - 1 = H_0(t_0 - t) + \frac{1}{2}(q_0 + 2)H_0^2(t_0 - t)^2 + \cdots \tag{3.9}$$

This can be inverted, to give the look-back time as a power series in the redshift:

$$H_0(t_0 - t) = z - \frac{1}{2}(q_0 + 2)z^2 + \cdots. \tag{3.10}$$

The coordinate distance r of the luminous object in a spatially flat universe (K=0) is given by

$$r = \int_t^{t_0} \frac{dt'}{a(t')} = \int_t^{t_0} \frac{dt'}{a(t_0)[1 + (t - t_0)H_0 - \frac{1}{2}(t - t_0)^2(q_0 H_0^2) + \cdots]} \tag{3.11}$$

which can be expanded as:

$$r + \cdots = \frac{t_0 - t}{a(t_0)} + \frac{H_0(t_0 - t)^2}{2a(t_0)} + \cdots \tag{3.12}$$

Then one can write

$$a(t_0) r H_0 = z - \frac{1}{2}(1 + q_0)z^2 + \cdots \tag{3.13}$$

substituting this equation in the expression of d_L that inferred from the relation between apparent and absolute luminosity, one gets:

$$d_L = a(t_0)r(1 + z) = \frac{1}{H_0}[z + \frac{1}{2}(1 - q_0)z^2 + \cdots] \tag{3.14}$$

Another way to calculate luminosity distance can be made by the expression of the radial coordinate $r(z)$ of a source observed as a function of the redshift. So

$$r(z) = \int \frac{dt}{a} = \int \frac{da}{a^2 H} = \int \frac{dz}{H(z)} \tag{3.15}$$

H(z) is the Hubble expansion rate as a function of redshift z, In the Standard Model H(z) is given by:

$$H(z) = H_0 E(z);\ E(z) = \sqrt{\Omega_\Lambda + \Omega_M(1 + z)^3 + \Omega_R(1 + z)^4} \tag{3.16}$$

$$r(z) = \int \frac{dz}{H_0\sqrt{\Omega_\Lambda + \Omega_M(1 + z)^3 + \Omega_R(1 + z)^4}} \tag{3.17}$$

In this case one can express the luminosity distance of a source observed with redshift z as:

$$d_L = r(z)(1 + z) = \frac{1 + z}{H_0} \int \frac{dz}{\sqrt{\Omega_\Lambda + \Omega_M(1 + z)^3 + \Omega_R(1 + z)^4}} = \frac{1 + z}{H_0} \int \frac{dz}{E(z)} \tag{3.18}$$

CHAPTER 4

BASIC NON-LOCAL MEASUREMENTS OF HUBBLE CONSTANT

4.1. Cosmic Microwave Background (CMB)

The very early universe was thermal bath containing photons, neutrinos, dark matter particles, protons, electrons, helium nuclei, and photons. During that time the radiation was in thermal equilibrium with the hot dense matter due to the very rapid collisions between photons and free electrons, where energetic photons rapidly ionized any hydrogen that produced. The recombination era started when the temperature of the expanding Universe had lowered enough for protons and electrons to form neutral hydrogen giving the cosmic microwave background (CMB) as photons flew freely across the Universe. This time is called the last scattering surface.

Studying CMB radiation is an effective technique for measuring the universe's geometry, matter composition, and primordial fluctuations. In this section, we aim to briefly relate the temperature inhomogeneity of light in acoustic oscillations of baryon-photon fluid before recombination to the CMB anisotropies observed at present. This will be done for the sake of completeness although this point is not directly related to the study of Hubble tension. As we will see later, Hubble constant H_0 is determined by studying the relation

$$\theta = \frac{r_s}{D_A} \text{ , where } \quad r_s = \int_{z_*}^{\infty} \frac{c_s dz}{H(z)} \quad \text{and} \quad D_A = \int_0^{z_*} \frac{dz}{H(z)} \tag{4.1}$$

It is evident from this equation that only the size of the sound horizon r_s and the cosmological model adopted is important in this context. On the other hand the evolution of the temperature inhomogeneity at the last scattering surface and at later times till the present do not affect these quantities. They only affect the final form of the anisotropy.

In Section 2.3 we have derived the equation for temperature inhomogeneities of photons in the photon-baryon fluid in the era before recombination. This inhomogeneity evolves due to some effects at the era of the last scattering and in the following era till the present which will be briefly summarized at the end of this section. The inhomogeneity

Θ is 3-dimensional. This inhomogeneity must be projected to the sphere of the observation at present. To this end, first the 3-diemnsional inhomogeneity must be expressed in terms of spherical harmonics. Any 3-dimensional function $\Theta(\boldsymbol{x}, \hat{\boldsymbol{p}}, \eta)$ may be expressed in terms of spherical harmonics as

$$\Theta(\boldsymbol{x}, \hat{\boldsymbol{p}}, \eta) = \sum_{l=1}^{\infty} \sum_{m=-l}^{l} a_{lm}(\boldsymbol{x}, \eta) Y_{lm}(\hat{\boldsymbol{p}}) \tag{4.2}$$

where $\hat{\boldsymbol{p}}$ is the incoming photons' direction and

$$a_{lm}(\boldsymbol{x}, \eta) = \int \frac{d^3k}{(2\pi)^3} e^{i\boldsymbol{k}\cdot\boldsymbol{x}} \int d\Omega \; Y^*_{lm}(\hat{\boldsymbol{p}}) \; \Theta(\boldsymbol{x}, \hat{\boldsymbol{p}}, \eta) \tag{4.3}$$

isotropy of CMB temperature implies

$$\langle a_{lm} a*_{l'm'} \rangle = \delta_{ll'} \delta_{mm'} C_l \tag{4.4}$$

$\Delta T(\hat{\boldsymbol{p}})$ or $\Theta(\boldsymbol{x}_0, \hat{\boldsymbol{p}}, \eta_0)$ is measured in the position of the observer and may be expressed in terms of spherical harmonics as

$$\frac{\Delta T(\hat{\boldsymbol{p}})}{T} = \Theta(\boldsymbol{x}_0, \hat{\boldsymbol{p}}, \eta_0) = \sum_{l=1}^{\infty} \sum_{m=-l}^{l} a_{lm}(\boldsymbol{x}, \eta_0) Y_l^m(\hat{\boldsymbol{p}}) \tag{4.5}$$

The two-point correlation function is an excellent way to quantify anisotropies in the CMB. It can be expressed as

$$\langle \frac{\Delta T(\hat{\boldsymbol{p}})}{T} \frac{\Delta T(\hat{\boldsymbol{p}}')}{T} \rangle = \sum_{lm} C_l Y_l^m(\hat{\boldsymbol{p}}) Y_l^m(\hat{\boldsymbol{p}}') = \sum_{l} C_l \left(\frac{2l+1}{4\pi} \right) \mathcal{P}_l(\hat{\boldsymbol{p}} \cdot \hat{\boldsymbol{p}}') \tag{4.6}$$

where we have replaced Θ by $\frac{\Delta T}{T}$ that corresponds to the temperature anisotropy at the present time at the location of Earth while we reserve Θ for temperature isotropy in general, especially at the era before recombination. Hence one can write

$$C_l = \frac{1}{4\pi} \int d^2\hat{n} d^2\hat{n}' \mathcal{P}_l(\hat{\boldsymbol{p}} \cdot \hat{\boldsymbol{p}}') \langle \frac{\Delta T(\hat{\boldsymbol{p}})}{T} \frac{\Delta T(\hat{\boldsymbol{p}}')}{T} \rangle \tag{4.7}$$

One must be cautious about an important point here, the physical meaning of the lower indices l here are not the same as the ones in (2.62). The ones in (2.62) correspond to the expansion of the inhomogeneity at era before the recombination while the one here corresponds to its decomposition on the sphere of observation at present. For example,Θ_0 also is expanded in terms of the spherical harmonics as in (4.5).

Note that,$\frac{\Delta T}{T}$ observed at present, in addition to the frozen inhomogeneities due to the baryon-photon oscillations, has also contributions from sources of anisotropy just before recombination and at the time of recombination or after the recombination till today.

We have not discussed these contributions to $\frac{\Delta T}{T}$ since they do not change the angular size of the sound horizon of the anisotropy due to the baryon-photon fluid oscillations that we use in (4.1), so they are not directly related to the Hubble tension. It will be enough to mention these sources of anisotropies briefly as [11, 30, 97]

1. Doppler Effect: results from variations in plasma velocity during the recombination.

2. Sachs-Wolfe effect which is the blueshift or redshift in temperature caused by variations in the gravitational potential at the time of recombination. In fact, the acoustic oscillations discussed above may be considered as initial conditions for the Sachs-Wolf effect [11, 82]

3. The integrated Sachs-Wolfe effect is the same as the Sachs-Wolfe effect but with time-dependent fluctuations between the recombination and the present time.

4. The Dipole Anisotropy: This is due to the overall redshift of the CMB radiation arising from the earth's motion with respect to CMB. In fact, this contribution is subtracted from the CMB data to find the true anisotropy.

5. The Sunyaev-Zel'dovich effect is an anisotropy resulting from photons being scattered by intergalactic electrons within galaxy clusters.

6. Silk Damping: This is the diffusion of photons from hotter regions to colder ones at the times before recombination. This is a small-scale effect due to the fact that the baryon-photon fluid, in fact, consists of particles i.e. baryons and photons which are separated from each other by some distance. In other words, it is due to the non-vanishing mean free path of the photons in their collisions with baryons.

There are also additional contributions to anisotropies, namely, polarization of CMB photons by intergalactic and inter-stellar dust [80], and weak lensing [30, 97].

4.2. Impact of the Value of H_0 on CMB measurements in the Context of the Standard Model

Acoustic oscillations affect CMB radiation and the distribution of baryons. Photons decouple at z_* while baryons decouple at z_d. What we may measure is θ which represents the effect of the acoustic oscillations either on CMB or on large-scale structure

(LSS). For CMB one can write

$$\theta = \frac{r_s}{D_A} \ , \text{ where } \ r_s = \int_{z_*}^{\infty} \frac{c_s dz}{H(z)} \ , \quad \text{and} \quad D_A = \int_0^{z_*} \frac{dz}{H(z)} \tag{4.8}$$

H for ΛCDM can be written in the form

$$H(z) = H_0 E(z) \ ; \quad E(z) = \sqrt{\Omega_\Lambda + \Omega_M (1+z)^3 + \Omega_R (1+z)^4} \tag{4.9}$$

At the first glimpse, it seems as if the effect of changing the Hubble constant would cancels out in the formula of θ, but actually one can see its effect by considering Saha equation [97]

$$X(1 + SX) = 1 \tag{4.10}$$

where $X \equiv \frac{n_p}{n_p + n_{1s}}$ and S can be expressed as

$$S = 1.747 \times 10^{-22} e^{157894/T} T^{3/2} \Omega_B h^2 \tag{4.11}$$

here T is the temperature in degrees Kelvin and h is the Hubble constant in units of 100 km/Mpc/s. As we can see from (4.11), when the Hubble constant increases the temperature must be decreased in order to have a fixed value of S. This means that actually changing the Hubble constant value will affect the temperature where the decoupling happened at which is related to the redshift, then z_* will also be affected. In other words, if we assume that at $X = \tilde{X}$ the decoupling happens at some fixed value of the temperature $\tilde{T}$. Then, changing the Hubble constant, changes $\tilde{T}$, this, in turn, changes the redshift of decoupling.

4.3. Baryon Acoustic Oscillations (BAO)

Baryon acoustic oscillations (BAO) are imprints of the density fluctuations of baryonic matter that are observed at the present time in large-scale structure. They are due to the sound waves in the baryon-photon plasma before recombination. After the decoupling of baryons and photons, these oscillations are frozen in inhomogeneities of baryon distribution that result in large-scale structures (such as galaxies) at present time. BAO matter clustering serves as a ”standard ruler” for the length scale in cosmology, just how supernovae offer a ”standard candle” for astronomical observations. The greatest distance that the acoustic waves could travel in the plasma before cooling to the point where they became neutral atoms and decoupled light, stopping the expansion of the plasma density waves and ”freezing” them in place, is what determines the length of this standard ruler. See Fig. 4.1

In BAO feature, perturbation is measured using galaxy correlations e.g. in the transverse direction to the line of sight, the observable is the angular size of the sound horizon at the "cosmic drag" epoch, or at the epoch of baryons decoupling. So that in BAO measurements of the Hubble constant, z_* in r_s is replaced by the redshift at baryon drag z_d in the r_d; and z_* in D_A in (4.8) by the redshift of the observed point (e.g. the galaxy) z_{obs}. That is $\theta_\perp^{BAO}$ reads

$$\theta_\perp^{BAO} = \frac{r_d}{D_A(z_{\text{obs}})}\,, \text{ where } \quad r_d = \int_{z_d}^{\infty} \frac{c_s dz}{H(z)}\,, \quad \text{and} \quad D_A(z_{\text{obs}}) = \int_0^{z_{\text{obs}}} \frac{dz}{H(z)} \tag{4.12}$$

Astronomical surveys measure $\theta_\perp^{BAO}$ while r_d and D_A are calculated by specifying the cosmological model i.e. H(z). In the standard calculations H(z) is taken to be that of the standard model of cosmology. The observations give $\theta_\perp^{BAO} = \frac{r_s}{D_A(z_{\text{obs}})}$. In fact, r_d corresponds to the radius of the universe at the time of baryons decoupling while it is a small portion of the sky today because the size of the horizon in a matter dominated universe increases. BAO observations assist cosmologists learn more about the nature of dark energy (which drives the universe's accelerated expansion) by restricting cosmological parameters.

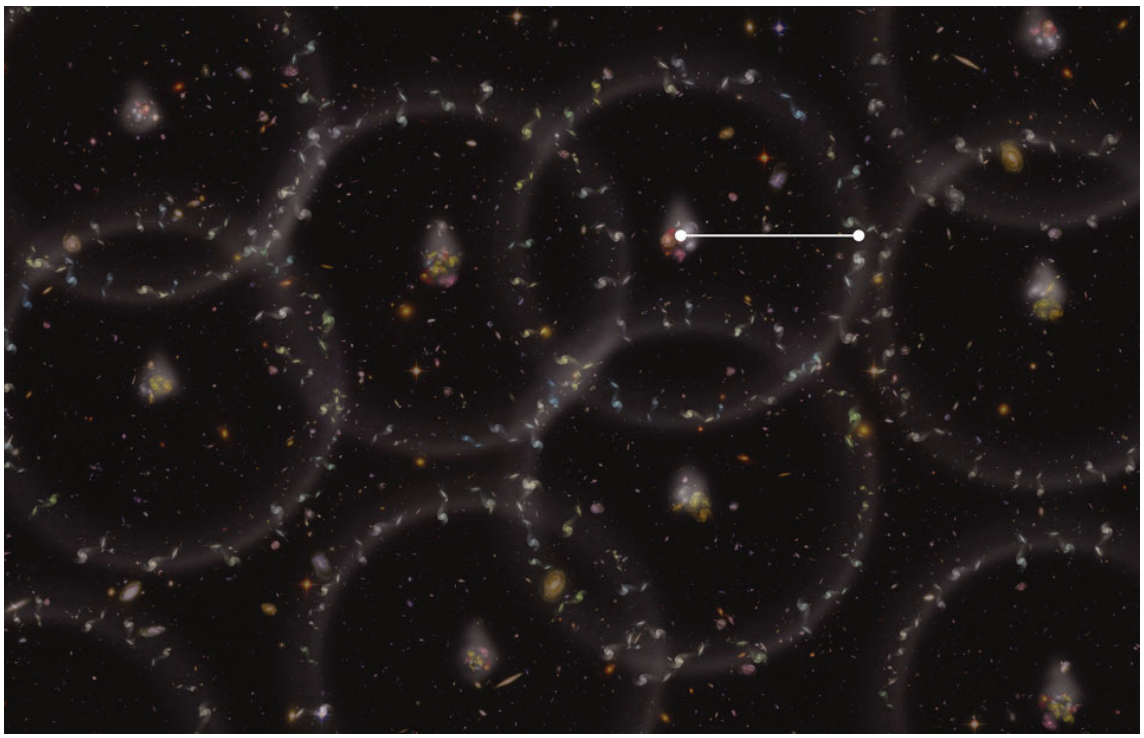

Figure 4.1. An artist's concept for a measurement of the universe's size. The gray spheres represent the pattern of BAO from the early Universe. Galaxies currently have a modest tendency to align with the spheres. This graphic shows an exaggerated alignment. Astronomers can calculate the distance between galaxies to within 1% accuracy by comparing the size of the spheres (white line) to the expected value. (Image Credit: Zosia Rostomian, Lawrence Berkeley National Laboratory, `https://newscenter.lbl.gov/2014/01/08/boss-one-percent/`)

CHAPTER 5

HUBBLE TENSION

Currently, there are multiple independent ways to infer the value of H_0. One method involves measuring the Hubble constant from the analysis of measurements of the cosmic microwave background (CMB) temperature and polarization spectra, another from the baryon acoustic oscillation (BAO) feature found in the large-scale distribution of galaxies after using the standard cosmological model (ΛCDM) in both methods. On the other hand, the Hubble constant can also be directly determined from measurements of distances to sufficiently distant luminous celestial objects such as Type Ia supernovae (SNe Ia). This approach relies on the absolute luminosity measurements of these SNe Ia that can be calibrated for example through measurements of Cepheids, which are variable stars known to exhibit periodic changes in brightness, which, in turn, are calibrated using geometry. This method is commonly referred to as the direct local measurements.

Estimates of the Hubble constant from local measurements are typically higher than those derived from CMB data, assuming the "standard" ΛCDM cosmological model. There is 4σ to 6σ discrepancy. The disagreement between the local and non-local measurements of H_0 is called Hubble tension[27, 75, 93].

To be more specific, let us discuss the problem in terms of equations. The (local) direct method of the determination of H_0 rely on measuring the luminosity distance d_L as a function of redshift z. As shown in the section 3.4 the luminosity distance at relatively small redshifts can be expressed as

$$d_L = \frac{1}{H_0}[z + \frac{1}{2}(1 - q_0)z^2 + \cdots] \tag{5.1}$$

where, q_0 is the deceleration parameter. We can measure the luminosity distance of supernovae for a set of low redshifts. q_0 is measured by Adam G. Riess and Louise Breuval [78] as $q_0 = -0.55$. Hence, we may determine H_0.

Another way to determine H_0 is the non-local methods such as CMB perturbations, BAO, etc. Both for CMB and BAO calculations [3, 4, 8, 66] a co-moving angle that is obtained from measurements are related to the co-moving sound horizon r_s and the co-moving distance D, that are calculated. For example, in the case of CMB perturbations we mainly measure the angular scale of perturbation on the last scattering surface θ_* that

is given by:

$$\theta_* = \frac{r_s}{D(z_*)} \text{ , where } r_s = \int_{z_*}^{\infty} \frac{c_s dz}{H(z)} \text{ and } D(z_*) = \int_0^{z_*} \frac{dz}{H(z)} \tag{5.2}$$

where in the case of ΛCDM

$$H(z) = H_0 E(z);\ E(z) = \sqrt{\Omega_\Lambda + \Omega_M (1+z)^3 + \Omega_R (1+z)^4} \tag{5.3}$$

Here, z_* is the redshift at which baryons and photons decouple, r_s is the sound horizon, which is the co-moving distance a sound wave may travel from the beginning of the universe till recombination, c_s is the baryon-photon sound speed, and $D(z_*)$ is the co-moving distance from a present-day observer to the last scattering surface. While c_s is mostly dependent on the baryon-to-photon ratio of energy densities as represented in (2.70), where R is supplied after (2.61), the value of z_* is substantially dictated by the measurement of the current CMB temperature and the standard atomic physics.

In the case of BAO, the perturbation is measured by using galaxy correlations in the transverse direction to the line of sight, the observable is the angular size of the sound horizon at the "cosmic drag" epoch, or at the epoch of baryon decoupling when measured today, $\theta_\perp^{BAO}$ that is given by

$$\theta_\perp^{BAO} = \frac{r_d}{D(z_{obs})} \text{ , where } r_d = \int_{z_d}^{\infty} \frac{c_s dz}{H(z)} \text{ and } D(z_{obs}) = \int_0^{z_{obs}} \frac{dz}{H(z)} \tag{5.4}$$

where z_{obs} is the redshift at which a given BAO measurement is made, r_d is the co-moving sound horizon at the end of the baryon drag epoch, and $D(z_{obs})$ is the co-moving distance from a present-day observer to the location of the perturbation.

Many studies have studied possible effects of measurement errors (i.e. systematics) in local mesurements of Hubble constant as a probable cause of the tension. These studies imply that the tension cannot be attributed to systematics [29, 42, 45, 76, 78]. Therefore, the most reasonable approach for the solution of this tension seems to be assuming that the local measurements correspond to the true value of H_0 and the non-local measurements may be brought to be in agreement with the CMB measurements by modifying ΛCDM by inclusion of new physics. This may be done in two different ways, namely, early time solutions and late time solutions.

5.1. The Basic Idea of Early Time Solutions

"Early" in this context refers to before the CMB photons last scattered, or during the first 400,000 years of the universe. Prior to the recombination phase (and after the time

of nucleosynthesis not to impact the successful outcome of the standard model), early time solutions alter the expansion history changing both H_0 and r_s in the appropriate direction (i.e. increasing H_0 while decreasing r_s so that both r_s and $D(z_*)$ decrease by the same amount) to solve the Hubble tension. Suppressing the extent of the sound horizon may be achieved most simply by raising the Hubble expansion rate during the pre-recombination era, which necessitates raising the energy density during that period.

One can see this point more clearly by considering the expression of the sound horizon in a spatially flat universe (K=0) i.e.

$$r_s = \int_{z_*}^{\infty} \frac{c_s dz}{H(z)} \tag{5.5}$$

and the co-moving distance to z_*

$$D(z_*) = \frac{1}{H_0} \int_0^{z_*} \frac{dz}{E(z)} \tag{5.6}$$

$$H(z) = H_0 E(z) \;\; ; \quad E(z) = \sqrt{\Omega_\Lambda + \Omega_M (1+z)^3 + \Omega_R (1+z)^4} \tag{5.7}$$

It is evident from (5.5) that larger energy gives smaller sound horizon. $E(z)$ is fixed in (5.6), while H_0 is increased. This, in turn, implies that $D(z_*)$ is decreased. One may decrease r_s and $D(z_*)$ by the same amount so that the angular scale of perturbation remains fixed:

$$\theta_* = \frac{r_s}{D(z_*)} \tag{5.8}$$

Workable solutions can be obtained by modifying ΛCDM at early times without affecting the successful predictions of the Standard Model such as nucleosynthesis. A viable approach is to propose a concept of "early dark energy" (EDE) that functions similarly to a cosmological constant before to matter-radiation equivalence but subsequently decays more quickly than radiation. This class of early time solutions seems to alleviate, but not to solve, the H_0 tension below the 3σ significance [29, 42, 66].

5.2. The Basic Idea of Late Time Solutions

Late time solutions of the Hubble constant tension are expansion history alterations following recombination that raise the H_0 value while maintaining the co-moving distance and the sound horizon unaltered. This means that, while maintaining the energy density as that of ΛCDM today, the energy density during periods between decoupling and now must be less than in the standard cosmological model. This then increases H_0 as is evident from (5.6). Then $\int_0^{z_*} \frac{dz}{E(z)}$ is greater when compared to the one for ΛCDM,

H_0 must increase by the same ratio. Therefore, the angular scale of perturbation (5.8) remains the same since r_s is unaltered in this solution.

This needs some exotic matter whose energy density grows with time concerning its standard form, given the reduction of the radiation and matter densities in a rising redshift. The simplest way to do this is to propose that a phantom-like fluid takes the place of the cosmological constant. i.e., a fluid with an equation of state

$$w = \frac{p}{\rho} < -1 \tag{5.9}$$

where p and ρ are here the dark-energy pressure and energy density.

CHAPTER 6

MAIN SCALAR FIELD MODELS PROPOSED FOR SOLUTION OF HUBBLE TENSION IN THE CONTEXT OF GENERAL RELATIVITY

6.1. General Aspects of Scalar Field Models

A "scalar field" is defined as a field that is invariant under Lorentz transformations. The energy density associated with particular scalar fields may be used to describe dark energy or dark matter in the scalar field model alternatives of the standard ΛCDM model [97]. For example, quintessence models are an example of such models [15, 98].

The general Lagrangian density of a scalar field ϕ is

$$\mathcal{L}_\phi = T(\phi) - V(\phi) = -\frac{1}{2}g^{\mu\nu}\partial_\mu\phi\partial_\nu\phi - V(\phi) \tag{6.1}$$

where $V(\phi)$ is an unspecified potential function, $T(\phi)$ is the kinetic energy, and g represents the determinant of RW metric. Hence, the action of such a scalar field can be expressed as

$$S_\phi = \int d^4x\sqrt{-g}\mathcal{L}_\phi = -\int d^4x\sqrt{-g}\left[\frac{1}{2}g^{\mu\nu}\partial_\mu\phi\partial_\nu\phi + V(\phi)\right] \tag{6.2}$$

One can use this action to write the corresponding energy-momentum tensor for scalar fields as

$$T_\phi^{\mu\nu} = -g^{\mu\nu}\left[\frac{1}{2}g^{\rho\sigma}\partial_\rho\phi\partial_\sigma\phi + V(\phi)\right] + g^{\mu\rho}g^{\nu\sigma}\partial_\rho\phi\partial_\sigma\phi \tag{6.3}$$

Let us now take a scalar field so that it depends on time only, not on position. Hence, energy density, pressure, and the equation of state may be expressed as

$$\rho_\phi = T_{00} = \frac{1}{2}\dot{\phi}^2 + V(\phi) \tag{6.4}$$

$$p_\phi = T_1^1 = T_2^2 = T_3^3 = \frac{1}{2}\dot{\phi}^2 - V(\phi) \tag{6.5}$$

$$w_\phi = \frac{p_\phi}{\rho_\phi} = \frac{\frac{1}{2}\dot{\phi}^2 - V(\phi)}{\frac{1}{2}\dot{\phi}^2 + V(\phi)} \tag{6.6}$$

Note that w_ϕ varies between -1 (that corresponds to the cosmological constant and is the case for $\dot{\phi}^2 << V(\phi)$) and 1 (that corresponds to stiff matter and is the case for $\dot{\phi}^2 >> V(\phi)$). In general, $-1 < w_\phi < 1$. The field equation obtained from the action (6.2) is

$$\nabla_\mu \nabla^\mu \phi + \frac{\partial V}{\partial \phi} = 0 \tag{6.7}$$

The equation of motion for $\phi = \phi(t)$ may be obtained from (6.7) or from(2.9), which reads

$$\ddot{\phi} + 3H\dot{\phi} + V'(\phi) = 0 \tag{6.8}$$

where $V'(\phi)$ is the derivative of $V(\phi)$ with respect to ϕ.

6.2. Late Time Solutions

In this class of models the evolution of $E(z) = H(z)/H_0$ in (5.7) is decreased in the era after decoupling so that $H(z)$ remains the same provided that H_0 may be increased to the value obtained from local measurements. This procedure does not change r_s. Hence, the value of the Hubble constant measured in local measurements may be fitted to the observed value of θ. We consider such three models to see the basic lines of this type of solutions in more detail.

6.2.1. Late dark energy transition

There are two types of late dark energy (LDE) transition models. One of them describes transitions from a matter-like to a cosmological constant behaviour at high redshifts after recombination. We will discuss this type of transition in the next section. In this section we will delve into the details of the second type which assume a late transition in the dark energy density near the present epoch. Such a transition is hidden from being observed by SNe Ia measurements if we take the redshift z_t (where the transition has taken place) to be smaller than the smallest redshifts of the observed supernovae. Only distance measurements below $z_t \lesssim 0.02$ would be sensitive to such a jump[10, 61]. This LDE modification of the ΛCDM expansion history leads to a fractional change of δ in the Hubble constant

$$H_0^2 = \tilde{H}_0^2(1 + 2\delta) \tag{6.9}$$

Here and throughout this section tildes denote values in a flat ΛCDM model with a cosmological constant density $\tilde{\rho}_\Lambda$. The basic idea of this model may be summarized as; H_0 in (6.9) may be considered as the true value of the Hubble constant measured by the direct local measurements while $\tilde{H}_0$ is close to the value measured by CMB and other non-local measurements. It is evident that this approach in principle may solve the Hubble tension in the view of the discussion in Section 5.2. The expression in (6.9) can be obtained from the limiting case of the following smooth dark energy density $\rho_{DE}(z)$

$$\rho_{DE}(z) = [1 + f(z)]\tilde{\rho}_\Lambda \tag{6.10}$$

Here, $f(z)$ is similar to a smooth step function that defined as

$$f(z) = \begin{cases} 0 & z \gg z_t \\ \frac{2\delta}{\tilde{\Omega}_\Lambda}\frac{S(z)}{S(0)} & \text{otherwise} \end{cases} \tag{6.11}$$

where

$$S(z) = \frac{1}{2}\left[1 - \tanh\left(\frac{z - z_t}{\Delta z}\right)\right] \tag{6.12}$$

In this definition, $z_t, \Delta z$ and δ are the position, width, and amplitude of the transition, respectively. the equation of state of the LDE model can be obtained by

$$1 + w = \frac{\dot{\rho}}{3H\rho} = \frac{1}{3}\frac{(1+z)f'}{1+f} \quad \text{where} \quad f' = \frac{df}{dz} \tag{6.13}$$

Now, to construct the scalar field model we identify the corresponding scalar field potential by using (6.4) and (6.5) as

$$V(z) = \frac{\rho_{DE} - p_{DE}}{2} = [(1 + f) - \frac{(1+z)f'}{6}]\tilde{\rho}_\Lambda \tag{6.14}$$

and the kinetic energy of the field can be expressed as

$$\frac{\dot{\phi}^2}{2} = \frac{\rho_{DE} + p_{DE}}{2} \tag{6.15}$$

So, one may obtain a scalar field that corresponds to (6.9).

$$\begin{aligned} \phi(z) = \int \dot{\phi}(z)dt &= \int_0^z |(1 + w(z'))\rho_{DE}(z')|^{1/2}\frac{dz'}{(1+z')H(z')} \\ &= \sqrt{\frac{\tilde{\rho}_\Lambda}{3}}\int_0^z \left(\frac{|f'|}{1+z'}\right)^{1/2}\frac{dz'}{H(z')} \end{aligned} \tag{6.16}$$

Although this model, in principle, can solve the Hubble tension as mentioned before, one cannot be sure if it really solves the tension because of the degeneracy between the Hubble constant and the supernovae absolute luminosities in the determination of the luminosity distances and the possibility of the variation of the absolute luminosities [10, 16] as may

be seen in the following formulas for apparent luminosity and the theoretical value of the luminosity distance

$$\ell = \frac{L}{4\pi d_L^2} = \frac{L}{4\pi \left(\frac{a_0(1+z)}{H_0} \int \frac{dz}{E(z)}\right)^2} \tag{6.17}$$

$$d_L = \frac{a_0(1+z)}{H_0} \int \frac{dz}{E(z)} \tag{6.18}$$

where $E(z)$ is given in (5.7).

Moreover, it is shown in [7] that this model should be supplemented by a transition in the absolute luminosities of the supernovas at a redshift of an order of 0.01 to solve the Hubble tension. A similar result is obtained in [38], which finds that BAO data favor an ultra-late-time (phantom-like) enhancement of $H(z)$ at $z < 0.2$ accompanied with a transition in the absolute magnitude of supernovae. However, a full CMB data analysis is currently missing [29]. On the other hand, it has been found that five different data-motivated priors of type Ia supernovae absolute magnitudes result in a range of H_0 that is compatible with both local and non-local measurements [21].

6.2.2. Late time transitions in the quintessence field

Probably the most popular cosmological scalar field model for dark energy and dark matter is quintessence. Therefore, [28] studied a quintessence field (a massive scalar field ϕ) that transitions from a matter-like to a cosmological constant behaviour at a late time to see if this model may solve the Hubble tension. In this model the transition is smooth and can be expressed by considering the effective equation of state:

$$w_{\phi\,\text{eff}}(a) = \frac{w_{\phi 0}}{1 + \left(\frac{a}{a_*}\right)^{-\frac{2}{\Delta}}} \tag{6.19}$$

where a_* is the scale factor at the time of transition, and Δ defines transition period. Then, using the continuity equation (2.11) the energy density in the quintessence field is depicted as

$$\rho_\phi = \rho_{\phi 0} \left(\frac{a}{a_0}\right)^{-3(1+w_{\phi 0})} \left[\frac{1 + \left(\frac{a_0}{a_*}\right)^{-\frac{2}{\Delta}}}{1 + \left(\frac{a}{a_*}\right)^{-\frac{2}{\Delta}}}\right]^{\frac{3\ \Delta\ w_{\phi 0}}{2}} \tag{6.20}$$

where a_0 and $\rho_{\phi 0}$ are the present value of the scale factor and of the energy density in quintessence, respectively.

The above phenomenological framework may be derived from the following scalar field model. The scalar field satisfies the Klein-Gordon equation

$$\ddot{\phi}+3H\dot{\phi}-\nabla^2\phi+m^2\phi+\frac{\partial V_{\text{osc}}}{\partial\phi}=0\ , \quad \text{where} \quad V_{\text{osc}}(\phi)=\Lambda^4\left[1-\cos\left(\frac{\phi}{f}\right)\right] \tag{6.21}$$

Λ is a free parameter which controls the height of the perturbations over the quadratic potential, and f is the energy scale that controls the field excursion.

Initially (at time of inflation), the Hubble parameter H is so large that only the first two terms in (6.21) contribute to the equation of motion with a constant ϕ as a solution. Later, H becomes very small compared to the mass term (and the other potential term which is much larger than the mass term). In this era, the scalar ϕ oscillates about a minimum of the potential with an effective equation of state 0 (i.e. the scalar behaves like matter). After that, the field tunnels to another minimum of the potential behaving as another fluid with equation of state $w_{\phi 0}$ (in particular, ϕ may take a constant value and behave like a cosmological constant with equation of state -1).

[28] investigated this extension of the ΛCDM model by using four different analyses. It showed that this model with changing only a_* does not help in relieving the Hubble constant tension. Also, in the case of letting f and Δ free to vary, because these parameters do not correlate with H_0, do not alleviate the tensions between Planck and the other cosmological probes. In the case of free dark energy equation of state also the case of free $w_{\phi 0}$ with the total neutrino mass $\sum m_\nu$ and the number of relativistic degrees of freedom N_{eff}, because of the strong anti-correlation between $w_{\phi 0}$ and H_0 also between $\sum m_\nu$ and H_0 in both cases [28] found a shift of the Hubble constant towards lower values, increasing the tension with Planck and the local measurements. [59] included curvature to extend the one-parameter and three-parameter parameterizations of [43] in the analysis and found that the H_0 tension remains above the 3σ.

6.2.3. Chameleon dark energy

A late-time inhomogeneous resolution is proposed by [12] suggesting that as an effective cosmological constant, a chameleon field coupled with a local overdensity of matter (since the physical characteristics of the chameleon field including its mass, are highly dependent on its surroundings, as it is a sort of scalar field that behaves quite differently in high-density areas than in low-density areas [50]) might be imprisoned at a greater potential energy density, accelerating the local expansion rate relative to the background with lower matter density.

The chameleon field ϕ introduces extra interactions with matter fields ψ_i with conformal factor $\Omega_i(\phi)$. The action for this model is given by

$$S = \int d^4x\sqrt{-g}\left(\frac{M_{Pl}^2}{2}R - \frac{1}{2}(\partial\phi)^2 - V(\phi)\right) + \sum_i S_m^{(i)}[\Omega_i^2(\phi)g_{\mu\nu}, \psi_i] \tag{6.22}$$

where M_{Pl} is is the reduced Planck mass. The metric employed in the first term in (6.22) i.e. in Hilbert-Einstein term and the chameleon action is $g_{\mu\nu}$ that is used in the Einstein frame metric. In this frame photons and baryons move on geodesics , while the metric for the $S_m^{(i)}$ terms is $\tilde{g}_{\mu\nu}$ which is induced by the chameleon coupling to matter and it is called Jordan-frame metric $\tilde{g}_{\mu\nu}^{(i)} = \Omega_i^2(\phi)g_{\mu\nu}$ in which DM moves on geodesics but photons and baryons are accelerated [48]. Therefore, chameleon has an effective potential V_{eff} that can be expressed as

$$V_{\text{eff}}(\phi) = V(\phi) + \Omega(\phi)\hat{\rho}_m \tag{6.23}$$

where $\hat{\rho}_m$ is the covariantly conserved energy density defined in Appendix B. The effective potential is the sum of two contributions: one from the actual potential $V(\phi)$, and the other from coupling of ϕ to the matter density $\Omega(\phi)$[1] where

$$V(\phi) = \alpha\Lambda^4\left(\frac{\Lambda}{\phi}\right)^n \quad , \quad \Omega(\phi) = e^{\left(\frac{\phi}{\Lambda}\right)} \tag{6.24}$$

Then, the vacuum-expectation value that corresponds to the minimum of the potential can be expressed as

$$\langle\phi\rangle = (1+n)\Lambda W\left[\frac{1}{1+n}\left(\frac{\hat{\rho}_m}{n\alpha\Lambda^4}\right)^{-\frac{1}{1+n}}\right] \tag{6.25}$$

where $W(z)$ is the Lambert function defined by $z = W(z)e^{W(z)}$, and hereafter the mass scale Λ^4 will be chosen as the current critical density $3M_{Pl}^2H_{\sim\text{CMB}}^2$. This model assumes an inhomogeneous profile for the local Hubble constant. The chameleon field coupling to the background region gives the Hubble constant $H_{\sim\text{CMB}}$, while its coupling to sufficiently dense region of the matter overdensity (so that the Friedmann equation could be applied) gives another value for the Hubble constant $H_{\sim\text{local}}$. The Friedmann equations for each case [12] are

$$3M_{Pl}^2H_{\sim\text{CMB}}^2 = \hat{\rho}_m^{\sim\text{CMB}} + V_{\text{eff}}(\langle\phi\rangle_{\sim\text{CMB}}; n, \alpha, \hat{\rho}_m^{\sim\text{CMB}}) \tag{6.26}$$

and

$$3M_{Pl}^2H_{\sim\text{local}}^2 = \hat{\rho}_m^{\sim\text{local}} + V_{\text{eff}}(\langle\phi\rangle_{\sim\text{local}}; n, \alpha, \hat{\rho}_m^{\sim\text{local}}) \tag{6.27}$$

[1]The uncoupled scalar field regime is recovered in the limit $\Omega_i(\phi) \to 0$.

namely

$$\frac{H^2_{\sim\text{local}}}{H^2_{\sim\text{CMB}}} = \frac{\hat{\rho}_m^{\sim\text{local}}}{\Lambda^4} + \alpha\left(\frac{\Lambda}{\langle\phi\rangle_{\sim\text{local}}}\right)^n + e^{\left(\frac{\langle\phi\rangle_{\sim\text{local}}}{\Lambda}\right)}\frac{\hat{\rho}_m^{\sim\text{local}}}{\Lambda^4} \tag{6.28}$$

with α solved by matching $H_{\sim\text{local}}$ to $H_{\sim\text{CMB}}$. As one can see from (6.28), by increasing $\langle\phi\rangle_{\sim\text{local}}$, $H_{\sim\text{local}}$ will be higher, explaining the local measurements of the Hubble constant. In this model it was found that 20% overdensity in the local region is sufficient to reproduce the local measurement on the Hubble constant [12]. But a full data analysis is however missing [29].

6.3. Early Time Solutions

In this class of models, the amount of energy before the recombination period is larger than the one in the ΛCDM model. Increasing $H(z)$ in r_s, increasing H_0 in $D(z_*)$ while keeping $E(z)$ fixed so that it results in smaller r_s and $D(z_*)$ with the angular scale of perturbation (5.8) remaining fixed. The observed value of θ may thus be matched to the value of the Hubble constant as determined in local measurements. We consider such three models to see the basic lines of this type of solutions in more detail.

6.3.1. Chameleon early dark energy

This model designates a cosmology called "chameleon EDE" or CEDE, that suggests EDE scalar field that couples to dark matter, inspired by chameleon models of dark energy [50], such that the dark matter becoming the dominant component of the Universe close to matter-radiation equality at z_{eq}. As we have demonstrated in section 6.2.3, such a connection results in a change in the scalar's effective potential as well as a modulation of the dark matter mass. The choices of scalar field potential and form of the coupling in [48] are

$$V(\phi) = \lambda\phi^4 \,, \;\; \Omega(\phi) = e^{\frac{\beta\phi}{M_{Pl}}} \tag{6.29}$$

where λ and β are dimensionless constants. Then the effective potential is

$$V_{\text{eff}}(\phi) = V(\phi) + \Omega(\phi)\rho_{dm} = \lambda\phi^4 + e^{\frac{\beta\phi}{M_{Pl}}}\rho_{dm} \tag{6.30}$$

Here, the fundamental Friedmann equation reads

$$3M_{Pl}^2H^2 = \frac{1}{2}\dot{\phi}^2 + V_{\text{eff}}(\phi) + \rho_m + \rho_\Lambda = \frac{1}{2}\dot{\phi}^2 + V(\phi) + \Omega(\phi)\rho_{dm} + \rho_m + \rho_\Lambda \tag{6.31}$$

where ρ_{dm} is the dark matter density. Thus, the contribution of dark matter (DM) to the overall energy supply of the universe at any given time is $\rho_{dm}\Omega(\phi)$, which may be seen as a modulation of the DM particle's mass. Therefore, the equation of motion of the scalar is modified by an additional source term dependent on the dark matter density i.e.

$$\ddot{\phi} + 3H\dot{\phi} + \frac{dV_{\text{eff}}(\phi)}{d\phi} = 0 \tag{6.32}$$

The coupling to DM most noticeably modifies the early-time behavior of the scalar field which can be seen at high redshifts in Fig. 6.1a. It acts like the cosmological constant and then it decays fast as a^{-4} and as DM dilutes away, the native potential of the scalar comes again into play. After the scalar Hubble frozen for some time, the scalar then begins to roll and oscillate asymmetrically in effective potential about a new, time-varying minimum. This shifts the odd (even) peaks in the fractional energy density to lower (higher) energy density than in the symmetric-potential uncoupled EDE case as shown in Fig. 6.1b. This model has the potential to solve Hubble tension. In particular, a potential ϕ^4 for CEDE can be used to refine the issue by adding an adjustable parameter, β as illustrated in Fig. 6.1a. However, full data analysis is missing for this model, and this seems to be a difficult task in view of the complicated form of the model [48].

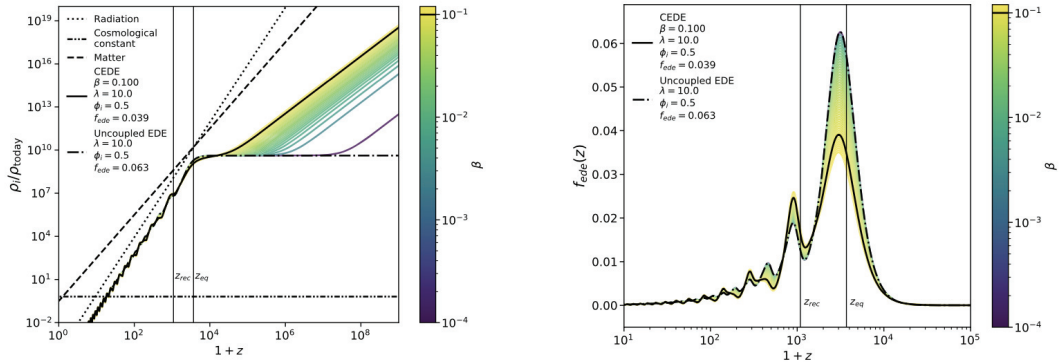

(a) Energy densities of various components of the Universe

(b) the fractional energy density f_{ede} in the EDE and CEDE scalar fields

Figure 6.1. The uncoupled EDE (dot-dashed) and CEDE (solid) models. Colors show the variation of ρ_{scf} with β [48]

6.3.2. New early dark energy

New early dark energy (NEDE) is a component of vacuum energy on the electron volt scale that decays in a first-order phase transition just before recombination [62]. According to NEDE, recombination in the early Universe is assumed to have preceded the vacuum first-order phase transition of the NEDE scalar field. In fact there are two types of new early dark energy models; cold new early dark energy and hot new early dark energy. Cold new early dark energy is an extension of early dark energy with addition of an extra scalar ϕ that triggers the increase and decrease of the energy density of the first scalar field ψ. In hot new early dark energy model the trigger field ϕ is replaced by temperature. Here we will consider the cold new dark energy model since the basic lines of models are the same. The first scalar ψ behaves as dark energy before its transition to an energy density that decays like radiation or faster. The NEDE abrupt transition may be expressed by a scalar field ψ whose potential at a critical point creates two non-degenerate minima (true and false vacuum) [66]. This can be achieved by considering a tunneling field ψ and an extra subdominant trigger field ϕ that, when activated, dramatically increases the tunneling rate.

This model has the form of general potential $V(\psi, \phi)$ as

$$V(\psi,\phi) = \frac{\lambda}{4}\psi^4 - \frac{1}{3}\alpha M\psi^3 + \frac{1}{2}\beta M^2\psi^2 + \frac{1}{2}m^2\phi^2 + \frac{1}{2}\tilde{\lambda}\phi^2\psi^2 \tag{6.33}$$

where $\alpha, \beta, \lambda,$ and $\tilde{\lambda}$ are positive, dimensionless constants, while M represents a general mass scale. It is advantageous to define a dimensionless potential or in other words rescale V by multiplying both sides of (6.33) by $\frac{81\lambda^3}{(\alpha^4 m^4)}$

$$\bar{V}(\bar{\psi},\bar{\phi}) = \frac{1}{4}\bar{\psi}^4 - \bar{\psi}^3 + \frac{\delta_{\text{eff}}(\bar{\phi})}{2}\bar{\psi}^2 + \frac{1}{2}\kappa^2\bar{\phi}^{\,2}\,, \quad \text{where } \kappa = \frac{3\lambda}{\alpha\sqrt{\tilde{\lambda}}}\frac{m}{M} \tag{6.34}$$

as we utilized the dimensionless variables $\bar{\psi} = \frac{3\lambda}{\alpha M}\psi$, and $\bar{\phi} = \frac{3\sqrt{\lambda\tilde{\lambda}}}{\alpha M}\phi$ as well as $\delta_{\text{eff}} = \delta + \bar{\phi}^{\,2} = 9\frac{\lambda\beta}{\alpha^2} + \bar{\phi}^{\,2}$ that controls the shape of the potential for the dimensionless tunneling field $\bar{\psi}$.

As shown in [63] ψ has two minima. ψ is at the false vacuum before the transition and it makes a fast tunneling to the true vacuum at the transition by the help of ϕ. The result is a sudden localized peak in the energy density of ϕ before recombination. This causes a localized energy density before recombination so that the sound horizon is decreases without spoiling the era of nucleosynthesis. In other words, it describes an almost instantaneous transition from a background fluid with an EoS parameter that varies from

-1 to w_{NEDE}

$$w_{\text{NEDE}}(t) = \begin{cases} -1 & \text{for } t < t_* \\ w^*_{\text{NEDE}} & \text{for } t > t_* \end{cases} \tag{6.35}$$

where the transition happens at time t_*.

In [63] it was shown that there exists a parameter space in this model where the time of the jump in the energy density of ψ may localized at the correct time with the correct magnitude so that it may resolve the Hubble tension. In [25], the effects of incorporating Atacama Cosmology Telescope (ACT) were investigated, yielding $H_0 = 71.49 \pm 0.822$ km/Mpc/s (68%C.L.) and a best-fit of $H_0 = 72.09$ km/Mpc/s. The model's fit quality in comparison to ΛCDM, notably improves, leading to a reduction in tension from 4.8σ down from 2.9σ within ΛCDM. However, the ACT data somewhat diminishes the efficiency of NEDE in addressing the Hubble tension. On the other hand, incorporating the South Pole Telescope (SPT) data resulted in $H_0 = 71.431 \pm 0.852$ km/Mpc/s (68% C.L.) and a best-fit of $H_0 = 71.77$ km/Mpc/s demonstrating a strong fit that reduces the tension to below 2σ. This model effectively decreases the Hubble tension from approximately 4.8σ to around 2σ establishing itself as one of the most promising solutions to the Hubble tension [23, 64, 84].

6.3.3. Anharmonic oscillations

Anharmonic oscillations model is one of EDE models that tries to reduce the H_0 tension [72]. This model's scalar field has a potential having an oscillating feature of the form [46]:

$$V_n(\phi) \propto \left(1 - \cos\frac{\phi}{f}\right)^n \tag{6.36}$$

The homogeneous Klein-Gordon equation of motion for the field is given by

$$\ddot{\phi} + 3H\dot{\phi} + \frac{dV_n(\phi)}{d\phi} = 0 \tag{6.37}$$

To see the physical implications of (6.36) more clearly, we may consider the case $n = 1$ [46]. One may take H very large initially so that the contribution of the potential to (6.37) is much smaller than the contribution of the second term. At this time $\phi =$ constant is a solution of (6.37). By (6.6), $\phi =$ constant corresponds to $w = -1$. We may let this correspond to the inflationary universe era. At this time, the time derivative of ϕ is zero. The later evolution may be either of the following two ways: 1- The field initially may be

at the maximum of the potential (that corresponds to $\phi/f = -\pi$), 2- The field may be at the minimum of the potential (that corresponds to $\phi/f = \pi$). In the first case, ϕ later gets smaller and behaves like dark energy. In the second case, ϕ is close to the minimum of the potential (that may correspond to the later evolution of the case -1). This corresponds to the time when the second term in (6.37) is negligible after a sufficiently long time when H gets sufficiently small.

In the case small ϕ/f, (6.36) may be approximated by

$$V_n(\phi) \propto \phi^{2n} \tag{6.38}$$

This results in the following equation of state [91]

$$w_n \equiv \frac{n-1}{n+1}. \tag{6.39}$$

where the replacements $\gamma = 1 + w, n \to 2n$ are done when compared to [91]. When the oscillations become rapid compared with the expansion rate, one can use the effective-fluid approximation [70] to find the scalar-field equations of motion. The scalar field initially (i.e. at very large z) has the equation of state of the cosmological constant, and at late times (i.e. at small z) behaves as a fluid with the equation of state given in (6.39). Therefore, The energy density parameter of the scalar field may be taken as:

$$\Omega_\phi(a) = \frac{2\Omega_\phi(a_c)}{(\frac{a}{a_c})^{3(w_n+1)} + 1} \tag{6.40}$$

which has an associated equation of state

$$w_\phi(z) = \frac{1+w_n}{1+(\frac{a}{a_c})^{-3(1+w_n)}} - 1 \tag{6.41}$$

It asymptotically approaches -1 as $a \to 0$ representing that the energy density is constant at early times while approaches w_n for $a \gg a_c$, showing that the energy density is diluted as $a^{-3(1+w_n)}$ when the scalar field becomes dynamical [79]. The homogeneous EDE energy density dilutes like matter for $(w_n = 0)\ n = 1$, like radiation for $(w_n = 1/3)\ n = 2$, and faster than radiation whenever $n \geq 3$. For $n \to \infty$ the scalar field is fully dominated by its kinetic energy $w_n \to 1$ and the energy density dilutes as a^{-6}. In [72], it was found that $n = 3$ is the solution preferred by the data used, gives $H_0 = 70.6 \pm 1.3$ km/Mpc/s at 68% CL, solving the Hubble tension within 2σ. This resolution requires a $\sim 5\%$ contribution from EDE to the total energy density at redshift $z \simeq 5000$ that then dilutes later[72].

CHAPTER 7

CONCLUSION

In this thesis, we have reviewed the concept of the Hubble constant tension and discussed some models that try to solve this tension in the context of scalar field models. We have given a brief overview of the standard model of cosmology discussing the background evolution using RW metric and deriving Friedmann equations, furthermore, exhibiting the cosmological perturbations for RW metric and Einstein field equations. We have also used the Boltzmann equation in order to derive the equation for the baryon-photon wave and show that this wave has sound speed c_s that depends on the universe's baryon density. We also have considered the Hubble constant determination techniques after presenting the main measurement methods used in cosmology to determine distances; the cosmic distance ladder for the local measurements, while CMB and BAO measurements for the non-local measurements of H_0. We also, for the sake of completeness, have considered the evolution of the inhomogeneities and the anisotropies at the present time.

In Chapter 5, we have discussed what is the Hubble tension and the basic ideas for its solution which are categorized as early and late time solutions. In the next chapter, we have given three models for each type of these solutions within the scalar field models. Regarding these six models that we considered, it seems that the late dark energy transition model should include a change in the absolute luminosities of supernovae at a redshift of roughly 0.01 [7]. However, no complete study of CMB data is yet available[29]. Late time transitions in the quintessence field model either by adjusting only a_* or allowing changes in f and Δ, do not help in relieving the Hubble tension, keeping it above the 3σ [28]. Introducing a variable equation of state for dark energy within this context shifts the Hubble constant towards lower values, exacerbating the Hubble tension [28]. In the late Chameleon dark energy model, studies have shown that 20% overdensity in the local region is sufficient to reproduce the local measurement on the Hubble constant [12]. In fact, [13] finds that late-time solutions are strongly disfavored if the late-time matter perturbation data are included. Chameleon early dark energy model has also the potential to solve Hubble tension [48]. However, for both of them, complete data analysis is still lacking [29]. New early dark energy model effectively decreases the Hubble tension from approximately 4.8σ to around 2σ establishing itself as one of the most promising

solutions to the Hubble tension [23, 25, 64, 84]. Anharmonic oscillation model requires a $\sim 5\%$ contribution from EDE to the total energy density at redshift $z \simeq 5000$ to solve the Hubble tension within 2σ [72]. CMB data from ACT shows a 3σ preference for EDE over ΛCDM, while it increases S_8 tension [73]. Also, in [40] it is found that early dark energy mitigates the tension to 3σ. [22] finds that one of the late time decaying dark matter cannot relieve the Hubble tension while some other models of this type like [24] are compatible with observations. The observational relevance of early dark energy models seems to be inconclusive, and the situation may be improved in the next generations of measurements [71].

In this thesis only some typical scalar filed models are considered. There are other scalar field models and non-scalar field models as well. However, the observational relevance of the models that are not discussed here is not much better than the ones discussed in this thesis. For example, there is no preference for interacting dark energy models over ΛCDM [41, 71, 92]. [56] finds that observational data disfavor self-interacting neutrino models (except possibly self-interacting tau neutrino models). [65] finds that extended interacting dynamical dark energy is very efficient in alleviating the Hubble tension. Axion-like early dark energy and the acoustic oscillation models seem not to be able to solve the tension while they are mitigating the tension [32, 86]. [6] considers a model where the cosmological constant changes sign from a negative cosmological constant to a positive one. They find that the Planck + BAOtr + PP data prefers this model over ΛCDM while it has a weak preference when only the Planck data is considered. The main problem with this model is the question of whether the sign flip in cosmological constant may be motivated by a concrete physical mechanism while there are proposals in this direction [5]. Time-varying electron mass solution to Hubble tension [85] is considered the best model that reduces the tension to the $\lesssim 2\sigma$ [84]. However, [49] finds that this model together with Majoron models are ruled out by data while time-varying electron mass solutions with spatial curvature and the early dark energy models reduce the tension to $1.0 - 2.9\sigma$ level, but none of these models is good enough to be the next model of Cosmology. Another study finds that the Hubble tension may be solved in the context of the Planck CMB data by modification of recombination while the inclusion of BAO and uncalibrated supernovae data makes the solution fully acceptable for perturbative modifications of recombination [53].

In conclusion, this thesis has discussed the Hubble tension and the proposed alternative models for resolving it within the context of scalar field theories. It seems that none of the models including the non-scalar ones are able to solve the Hubble tension although

some of them mitigate it.

APPENDIX A

DERIVATION OF ROBERTSON-WALKER METRIC

In this appendix we will derive Robertson-Walker Metric relying solely on the assumption of homogeneity and isotropy. The symmetries present in the Cosmological Principle require a constant lapse function, g_{tt} . The differential distance formula [18, 96], or metric consistent with the Cosmological Principle and Weyl's postulate is

$$ds^2 \equiv g_{\mu\nu}dx^\mu dx^\nu = -dt^2 + a^2(t)d\sigma^2 \tag{A.1}$$

where t is timelike coordinate, $a(t)$ is a function known as the scale factor, and $d\sigma^2$ is the general 3-dimensional spherically symmetric matrix that can be expressed as [96]

$$d\sigma^2 \equiv g_{ij}dx^i dx^j = A(r)dr^2 + r^2\left(d\theta^2 + \sin^2\theta d\phi^2\right) \tag{A.2}$$

we may set $A(r) = e^{2\beta(r)}$. The corresponding Ricci tensors can be written as:

$$\begin{aligned} R_{rr} &= \frac{2}{r}\partial_r\beta(r) \\ R_{\theta\theta} &= e^{-2\beta}(r\partial_r\beta(r) - 1) + 1 \\ R_{\phi\phi} &= [e^{-2\beta}(r\partial_r\beta(r) - 1) + 1]\sin^2\theta \end{aligned} \tag{A.3}$$

It may be shown that the isotropy and the homogeneity of universe implies that the space-time can be decomposed into maximally symmetric subspaces [96]. We know that maximally symmetric metrics obey[18]

$$R_{\mu\nu} = (n-1)kg_{\mu\nu} \tag{A.4}$$

where k known as the curvature constant and can be expressed as

$$k = \begin{cases} +1 & \text{for the spherical space} \\ -1 & \text{for the hyperbolic space} \\ 0 & \text{for the flat space} \end{cases} \tag{A.5}$$

In this case $n = 3$, then

$$R_{rr} = 2ke^{2\beta}\ , \quad R_{\theta\theta} = 2kr^2\ , \quad R_{\phi\phi} = 2kr^2\sin^2\theta \tag{A.6}$$

Now, we equate (A.3) to (A.6) and solve the equation to find β

$$\beta = -\frac{1}{2} \ln 1 - kr^2 \tag{A.7}$$

Thus we obtain the explicit form of (A.1) as

$$ds^2 = -dt^2 + a^2(t) \left(\frac{dr^2}{1 - kr^2} + r^2 d\theta^2 + r^2 \sin^2 \theta d\phi^2 \right) \tag{A.8}$$

This metric (A.8) is known in cosmology as the Robertson-Walker metric which was first rigorously derived in the 1930's by Howard Percy Robertson [81] and (independently) Arthur Geoffrey Walker [94], and is commonly referred to as the Robertson-Walker metric which is considered as the backbone of standard cosmology.

APPENDIX B

DERIVATION OF $\hat{\rho}$ IN CHAMELEON DARK ENERGY

The chameleon field ϕ introduces extra interactions with matter fields ψ_i with conformal factor $\Omega_i(\phi)$. In Jordan-frame, the corresponding energy-momentum tensor $\tilde{T}^{\mu\nu}_{(i)}$ is conserved by $\tilde{\nabla}^{(i)}_{\mu}\tilde{T}^{\mu\nu}_{(i)} = 0$ while in Einstein frame the energy-momentum tensor $T^{\mu\nu}_{(i)}$, in this case, is not conserved, but one can get the relation between these from the action variation in both frames as $\tilde{T}^{\mu\nu}_{(i)}\Omega_i^6(\phi) = T^{\mu\nu}_{(i)}$ [14]. Then, express the conservation relation in the Jordan frame using Einstein's frame of the energy-momentum tensor as

$$\tilde{\nabla}^{(i)}_{\mu}\tilde{T}^{\mu\nu}_{(i)} = \Omega_i^{-6}\nabla_\mu T^{\mu\nu}_{(i)} - T_i\Omega_i^{-7}\nabla^\nu\Omega_i = 0 \quad \rightarrow \quad \nabla_\mu T^{\mu}_{(i)\nu} = T_i\Omega_i^{-1}\nabla^\nu\Omega_i \tag{B.1}$$

with trace $T_i = \tilde{T}^{(i)}_{\mu\nu}\tilde{g}^{\mu\nu}_{(i)}$. Using a perfect fluid in Minkowski space the energy-momentum tensor (2.6) becomes $T^{\mu}_{(i)\nu} = \text{diag}(-\rho_i, p_i, p_i, p_i)$ with EoS (2.10), the $\nu = 0$ component of (B.1) reads

$$\nabla_t(\Omega_i^{3w_i-1}\rho_i) = 0 \tag{B.2}$$

This defines a covariantly conserved density $\hat{\rho}_i$

$$\hat{\rho}_i = \Omega_i^{3w_i-1}\rho_i = \Omega_i^{3w_i+3}\tilde{\rho}_i \tag{B.3}$$

BIBLIOGRAPHY

[1] Aaronson, M., J. Huchra, and J. Mould (1979). The infrared luminosity/hi velocity-width relation and its application to the distance scale. *Astrophysical Journal, Part 1, vol. 229, Apr. 1, 1979, p. 1-13. 229*, 1–13.

[2] Adil, S. A., O. Akarsu, E. Di Valentino, R. C. Nunes, E. Özülker, A. A. Sen, and E. Specogna (2024, Jan). Omnipotent dark energy: A phenomenological answer to the hubble tension. *Phys. Rev. D 109*, 023527.

[3] Aghanim, N., Y. Akrami, M. Ashdown, J. Aumont, C. Baccigalupi, M. Ballardini, A. Banday, R. Barreiro, N. Bartolo, S. Basak, et al. (2020). Planck 2018 results-vi. cosmological parameters. *Astronomy & Astrophysics 641*, A6.

[4] Aghanim, N., Y. Akrami, M. Ashdown, J. Aumont, C. Baccigalupi, M. Ballardini, A. Banday, R. B. Barreiro, N. Bartolo, S. Basak, et al. (2017). Planck intermediate results-li. features in the cosmic microwave background temperature power spectrum and shifts in cosmological parameters. *Astronomy & Astrophysics 607*, A95.

[5] Akarsu, O., A. De Felice, E. Di Valentino, S. Kumar, R. C. Nunes, E. Ozulker, J. A. Vazquez, and A. Yadav (2024). Λ_sCDM cosmology from a type-II minimally modified gravity. *arXiv preprint arXiv:2402.07716*.

[6] Akarsu, O., E. Di Valentino, S. Kumar, R. C. Nunes, J. A. Vazquez, and A. Yadav (2023, 7). Λ_sCDM model: A promising scenario for alleviation of cosmological tensions. *arXiv preprint arXiv: 2307.10899*.

[7] Alestas, G., L. Kazantzidis, and L. Perivolaropoulos (2021). w- m phantom transition at z t¡ 0.1 as a resolution of the hubble tension. *Physical Review D 103*(8), 083517.

[8] Anchordoqui, L. A., E. Di Valentino, S. Pan, and W. Yang (2021). Dissecting the H_0 and S_8 tensions with Planck+ BAO+ supernova type Ia in multi-parameter cosmologies. *Journal of High Energy Astrophysics 32*, 28–64.

[9] Baumann, D. (2021). Advanced cosmology lecture notes. *url: http://cosmology.*

amsterdam/education/advanced-cosmology.

[10] Benevento, G., W. Hu, and M. Raveri (2020). Can late dark energy transitions raise the hubble constant? *Physical Review D 101*(10), 103517.

[11] Bucher, M. (2015). Physics of the cosmic microwave background anisotropy. *Int. J. Mod. Phys. D 24*(02), 1530004.

[12] Cai, R.-G., Z.-K. Guo, L. Li, S.-J. Wang, and W.-W. Yu (2021). Chameleon dark energy can resolve the hubble tension. *Physical Review D 103*(12), L121302.

[13] Cai, R.-G., Z.-K. Guo, S.-J. Wang, W.-W. Yu, and Y. Zhou (2022, Sep). No-go guide for late-time solutions to the hubble tension: Matter perturbations. *Phys. Rev. D 106*, 063519.

[14] Cai, R.-G. and S.-J. Wang (2021). Higgs chameleon. *Physical Review D 103*(2), 023502.

[15] Caldwell, R. R., R. Dave, and P. J. Steinhardt (1998, Feb). Cosmological imprint of an energy component with general equation of state. *Phys. Rev. Lett. 80*, 1582–1585.

[16] Camarena, D. and V. Marra (2021). On the use of the local prior on the absolute magnitude of type ia supernovae in cosmological inference. *Monthly Notices of the Royal Astronomical Society 504*(4), 5164–5171.

[17] Capozziello, S., G. Sarracino, and G. De Somma (2024). A Critical Discussion on the H_0 Tension †. *Universe 10*(3), 140.

[18] Carroll, S. M. (2019). *Spacetime and geometry*. Cambridge University Press.

[19] Cervantes-Cota, J. L., S. Galindo-Uribarri, and G. F. Smoot (2023). The unsettled number: Hubble's tension. *Universe*.

[20] Chan, M. H. (2023). The cosmological ultra-low frequency radio background: a solution to the Hubble tension and the 21-cm excess trough. *Eur. Phys. J. C 83*(6), 509.

[21] Chen, Y., S. Kumar, B. Ratra, and T. Xu (2024). Effects of Type Ia Supernovae Ab-

solute Magnitude Priors on the Hubble Constant Value. *Astrophys. J. Lett. 964*(1), L4.

[22] Clark, S. J., K. Vattis, and S. M. Koushiappas (2021, Feb). Cosmological constraints on late-universe decaying dark matter as a solution to the H_0 tension. *Phys. Rev. D 103*, 043014.

[23] Cruz, J. S., S. Hannestad, E. B. Holm, F. Niedermann, M. S. Sloth, and T. Tram (2023). Profiling cold new early dark energy. *arXiv preprint arXiv:2302.07934*.

[24] Cruz, J. S., F. Niedermann, and M. S. Sloth (2023a, nov). Cold new early dark energy pulls the trigger on the H_0 and S_8 tensions: a simultaneous solution to both tensions without new ingredients. *Journal of Cosmology and Astroparticle Physics 2023*(11), 033.

[25] Cruz, J. S., F. Niedermann, and M. S. Sloth (2023b). A grounded perspective on new early dark energy using act, spt, and bicep/keck. *Journal of Cosmology and Astroparticle Physics 2023*(02), 041.

[26] Dainotti, M., B. De Simone, G. Montani;, T. Schiavone;, and G. Lambiase. (2023). The Hubble constant tension: current status and future perspectives through new cosmological probes. *PoS CORFU2022*, 235.

[27] Di Valentino, E. (2021). A combined analysis of the H_0 late time direct measurements and the impact on the dark energy sector. *Monthly Notices of the Royal Astronomical Society 502*(2), 2065–2073.

[28] Di Valentino, E., R. Z. Ferreira, L. Visinelli, and U. Danielsson (2019). Late time transitions in the quintessence field and the H_0 tension. *Physics of the Dark Universe 26*, 100385.

[29] Di Valentino, E., O. Mena, S. Pan, L. Visinelli, W. Yang, A. Melchiorri, D. F. Mota, A. G. Riess, and J. Silk (2021). In the realm of the hubble tension—a review of solutions. *Classical and Quantum Gravity 38*(15), 153001.

[30] Dodelson, S. and F. Schmidt (2020). *Modern cosmology*. Academic press.

[31] Dressler, A., D. Lynden-Bell, D. Burstein, R. L. Davies, S. Faber, R. Terlevich, and G. Wegner (1987). Spectroscopy and photometry of elliptical galaxies. i-a new distance estimator. *Astrophysical Journal, Part 1 (ISSN 0004-637X), vol. 313, Feb. 1, 1987, p. 42-58. 313*, 42–58.

[32] Efstathiou, G., E. Rosenberg, and V. Poulin (2023, 11). Improved Planck constraints on axion-like early dark energy as a resolution of the Hubble tension.

[33] Faber, S. and R. E. Jackson (1976). Velocity dispersions and mass-to-light ratios for elliptical galaxies. *Astrophysical Journal, vol. 204, Mar. 15, 1976, pt. 1, p. 668-683. 204*, 668–683.

[34] Freedman, W. L. and B. F. Madore (2010). The Hubble Constant. *Ann. Rev. Astron. Astrophys. 48*, 673–710.

[35] Freedman, W. L., B. F. Madore, T. Hoyt, I. S. Jang, R. Beaton, M. G. Lee, A. Monson, J. Neeley, and J. Rich (2020). Calibration of the tip of the red giant branch. *The Astrophysical Journal 891*(1), 57.

[36] Friedman, A. (1922). On the Curvature of space. *Z. Phys. 10*, 377–386.

[37] Gangopadhyay, M. R., S. K. J. Pacif, M. Sami, and M. K. Sharma (2023). Generic Modification of Gravity, Late Time Acceleration and Hubble Tension. *Universe 9*(2), 83.

[38] Gómez-Valent, A., A. Favale, M. Migliaccio, and A. A. Sen (2024, Jan). Late-time phenomenology required to solve the H_0 tension in view of the cosmic ladders and the anisotropic and angular bao datasets. *Phys. Rev. D 109*, 023525.

[39] Graczyk, D., G. Pietrzyński, I. B. Thompson, W. Gieren, B. Zgirski, S. Villanova, M. Górski, P. Wielgórski, P. Karczmarek, W. Narloch, et al. (2020). A distance determination to the small magellanic cloud with an accuracy of better than two percent based on late-type eclipsing binary stars. *The Astrophysical Journal 904*(1), 13.

[40] Gsponer, R., R. Zhao, J. Donald-McCann, D. Bacon, K. Koyama, R. Crittenden, T. Simon, and E.-M. Mueller (2023, 12). Cosmological constraints on early dark energy from the full shape analysis of eBOSS DR16.

[41] Hoerning, G. A., R. G. Landim, L. O. Ponte, R. P. Rolim, F. B. Abdalla, and E. Abdalla (2023, 8). Constraints on interacting dark energy revisited: implications for the Hubble tension.

[42] Hu, J.-P. and F.-Y. Wang (2023). Hubble tension: The evidence of new physics. *Universe 9*(2), 94.

[43] Huang, Z., J. R. Bond, and L. Kofman (2010, dec). Parameterizing and measuring dark energy trajectories from late inflatons. *The Astrophysical Journal 726*(2), 64.

[44] Hubble, E. (1929). A relation between distance and radial velocity among extragalactic nebulae. *Proceedings of the national academy of sciences 15*(3), 168–173.

[45] Huterer, D. (2023). Hubble tension. *Eur. Phys. J. Plus 138*(11), 1004.

[46] Kamionkowski, M., J. Pradler, and D. G. E. Walker (2014, Dec). Dark energy from the string axiverse. *Phys. Rev. Lett. 113*, 251302.

[47] Kamionkowski, M. and A. G. Riess (2023). The hubble tension and early dark energy. *Annual Review of Nuclear and Particle Science 73*, 153–180.

[48] Karwal, T., M. Raveri, B. Jain, J. Khoury, and M. Trodden (2022). Chameleon early dark energy and the hubble tension. *Physical Review D 105*(6), 063535.

[49] Khalife, A. R., M. B. Zanjani, S. Galli, S. Günther, J. Lesgourgues, and K. Benabed (2023, 12). Review of Hubble tension solutions with new SH0ES and SPT-3G data.

[50] Khoury, J. and A. Weltman (2004). Chameleon cosmology. *Physical Review D 69*(4), 044026.

[51] Krishnan, C., E. O. Colgáin, Ruchika, A. A. Sen, M. M. Sheikh-Jabbari, and T. Yang (2020, Nov). Is there an early universe solution to hubble tension? *Phys. Rev. D 102*, 103525.

[52] Leavitt, H. S. and E. C. Pickering (1912, March). Periods of 25 Variable Stars in the Small Magellanic Cloud. *Harvard College Observatory Circular 173*, 1–3.

[53] Lee, N., Y. Ali-Haïmoud, N. Schöneberg, and V. Poulin (2023, Apr). What it takes to solve the hubble tension through modifications of cosmological recombination. *Phys. Rev. Lett. 130*, 161003.

[54] Lemaitre, G. (1927). A Homogeneous Universe of Constant Mass and Growing Radius Accounting for the Radial Velocity of Extragalactic Nebulae. *Annales Soc. Sci. Bruxelles A 47*, 49–59.

[55] Li, X. and A. Shafieloo (2019, sep). A simple phenomenological emergent dark energy model can resolve the hubble tension. *The Astrophysical Journal Letters 883*(1), L3.

[56] Lyu, K.-F., E. Stamou, and L.-T. Wang (2021, Jan). Self-interacting neutrinos: Solution to hubble tension versus experimental constraints. *Phys. Rev. D 103*, 015004.

[57] Mazurenko, S., I. Banik, P. Kroupa, and M. Haslbauer (2024, January). A simultaneous solution to the hubble tension and observed bulk flow within $250h^{-1}$ mpc. *Monthly Notices of the Royal Astronomical Society 527*(3), 4388–4396. Funding: IB was supported by Science and Technology Facilities Council grant ST/V000861/1. PK thanks the Deutscher Akademischer Austauschdienst-Eastern European exchange programme for support.

[58] Melia, F. (2020). *The Cosmic Spacetime*. CRC Press.

[59] Miao, H. and Z. Huang (2018). The H_0 tension in non-flat QCDM cosmology. *The Astrophysical Journal 868*(1), 20.

[60] Monjo, R. and R. Campoamor-Stursberg (2023, aug). Geometric perspective for explaining hubble tension: theoretical and observational aspects. *Classical and Quantum Gravity 40*(19), 195006.

[61] Mortonson, M., W. Hu, and D. Huterer (2009, Sep). Hiding dark energy transitions at low redshift. *Phys. Rev. D 80*, 067301.

[62] Niedermann, F. and M. S. Sloth (2020, Sep). Resolving the hubble tension with new early dark energy. *Phys. Rev. D 102*, 063527.

[63] Niedermann, F. and M. S. Sloth (2021, Feb). New early dark energy. *Phys. Rev. D 103*,

L041303.

[64] Niedermann, F. and M. S. Sloth (2023). New early dark energy as a solution to the H_0 and S_8 tensions. *arXiv preprint arXiv:2307.03481*.

[65] Pan, S., W. Yang, E. Di Valentino, E. N. Saridakis, and S. Chakraborty (2019, Nov). Interacting scenarios with dynamical dark energy: Observational constraints and alleviation of the H_0 tension. *Phys. Rev. D 100*, 103520.

[66] Perivolaropoulos, L. and F. Skara (2022). Challenges for ΛCDM: An update. *New Astronomy Reviews 95*, 101659.

[67] Perryman, M. A., L. Lindegren, J. Kovalevsky, E. Hoeg, U. Bastian, P. Bernacca, M. Crézé, F. Donati, M. Grenon, M. Grewing, et al. (1997). The hipparcos catalogue. *Astronomy and Astrophysics, Vol. 323, p. L49-L52 323*, L49–L52.

[68] Pesce, D., J. Braatz, M. Reid, A. Riess, D. Scolnic, J. Condon, F. Gao, C. Henkel, C. Impellizzeri, C. Kuo, et al. (2020). The megamaser cosmology project. xiii. combined hubble constant constraints. *The Astrophysical Journal Letters 891*(1), L1.

[69] Pietrzyński, G., D. Graczyk, A. Gallenne, W. Gieren, I. Thompson, B. Pilecki, P. Karczmarek, M. Górski, K. Suchomska, M. Taormina, et al. (2019). A distance to the large magellanic cloud that is precise to one per cent. *Nature 567*(7747), 200–203.

[70] Poulin, V., T. L. Smith, D. Grin, T. Karwal, and M. Kamionkowski (2018, Oct). Cosmological implications of ultralight axionlike fields. *Phys. Rev. D 98*, 083525.

[71] Poulin, V., T. L. Smith, and T. Karwal (2023). The ups and downs of early dark energy solutions to the hubble tension: a review of models, hints and constraints circa 2023. *arXiv preprint arXiv:2302.09032*.

[72] Poulin, V., T. L. Smith, T. Karwal, and M. Kamionkowski (2019, Jun). Early dark energy can resolve the hubble tension. *Phys. Rev. Lett. 122*, 221301.

[73] Rebouças, J., J. Gordon, D. H. de Souza, K. Zhong, V. Miranda, R. Rosenfeld, T. Eifler, and E. Krause (2024). Early dark energy constraints with late-time expansion marginalization. *Journal of Cosmology and Astroparticle Physics 2024*(02), 042.

[74] Reid, M., D. W. Pesce, and A. Riess (2019). An improved distance to ngc 4258 and its implications for the hubble constant. *The Astrophysical Journal Letters 886*(2), L27.

[75] Riess, A. G. (2020). The expansion of the universe is faster than expected. *Nature Reviews Physics 2*(1), 10–12.

[76] Riess, A. G., G. S. Anand, W. Yuan, S. Casertano, A. Dolphin, L. M. Macri, L. Breuval, D. Scolnic, M. Perrin, and R. I. Anderson (2023, oct). Crowded no more: The accuracy of the hubble constant tested with high-resolution observations of cepheids by jwst. *The Astrophysical Journal Letters 956*(1), L18.

[77] Riess, A. G., G. S. Anand, W. Yuan, S. Casertano, A. Dolphin, L. M. Macri, L. Breuval, D. Scolnic, M. Perrin, and R. I. Anderson (2024, feb). Jwst observations reject unrecognized crowding of cepheid photometry as an explanation for the hubble tension at 8σ confidence. *The Astrophysical Journal Letters 962*(1), L17.

[78] Riess, A. G. and L. Breuval (2023, 8). The Local Value of H_0.

[79] Riess, A. G., L.-G. Strolger, J. Tonry, S. Casertano, H. C. Ferguson, B. Mobasher, P. Challis, A. V. Filippenko, S. Jha, W. Li, et al. (2004). Type ia supernova discoveries at z¿ 1 from the hubble space telescope: Evidence for past deceleration and constraints on dark energy evolution. *The Astrophysical Journal 607*(2), 665.

[80] Ritacco, A., F. Boulanger, V. Guillet, J.-M. Delouis, J.-L. Puget, J. Aumont, and L. Vacher (2023). Dust polarization spectral dependence from planck hfi data-turning point for cosmic microwave background polarization-foreground modeling. *Astronomy & Astrophysics 670*, A163.

[81] Robertson, H. P. (1935). Kinematics and world-structure. *Astrophysical Journal, vol. 82, p. 284 82*, 284.

[82] Sachs, R. K. and A. M. Wolfe (1967). Perturbations of a cosmological model and angular variations of the microwave background. *Astrophys. J. 147*, 73–90.

[83] Schmidt, B. P. (2012). Nobel Lecture: Accelerating expansion of the Universe through observations of distant supernovae. *Rev. Mod. Phys. 84*, 1151–1163.

[84] Schöneberg, N., G. Franco Abellán, A. Pérez Sánchez, S. J. Witte, V. Poulin, and J. Lesgourgues (2022). The H_0 Olympics: A fair ranking of proposed models. *Phys. Rept. 984*, 1–55.

[85] Seto, O. and Y. Toda (2023, Apr). Big bang nucleosynthesis constraints on varying electron mass solution to the hubble tension. *Phys. Rev. D 107*, 083512.

[86] Simon, T. (2023, 10). Can acoustic early dark energy still resolve the Hubble tension?

[87] Soltis, J., S. Casertano, and A. G. Riess (2021). The parallax of ω centauri measured from gaia edr3 and a direct, geometric calibration of the tip of the red giant branch and the hubble constant. *The Astrophysical Journal Letters 908*(1), L5.

[88] Testa, V., A. Chieffi, M. Limongi, G. Andreuzzi, and G. Marconi (2004). The distance to ngc 5904 (m 5) via the subdwarf main sequence fitting method. *Astronomy & Astrophysics 421*(2), 603–612.

[89] Tully, R. B. (2023). The hubble constant: A historical review. *arXiv preprint arXiv:2305.11950*.

[90] Tully, R. B. and J. R. Fisher (1977). A new method of determining distances to galaxies. *Astronomy and Astrophysics, vol. 54, no. 3, Feb. 1977, p. 661-673. 54*, 661–673.

[91] Turner, M. S. (1983). Coherent scalar-field oscillations in an expanding universe. *Physical Review D 28*(6), 1243.

[92] Vagnozzi, S. (2023). Seven Hints That Early-Time New Physics Alone Is Not Sufficient to Solve the Hubble Tension. *Universe 9*(9), 393.

[93] Verde, L., T. Treu, and A. G. Riess (2019). Tensions between the early and late universe. *Nature Astronomy 3*(10), 891–895.

[94] Walker, A. G. (1937). On milne's theory of world-structure. *Proceedings of the London Mathematical Society 2*(1), 90–127.

[95] Wang, D. (2023). Pantheon+ tomography and hubble tension. *The European Physical Journal C 83*(9), 813.

[96] Weinberg, S. (1972). *Gravitation and cosmology: principles and applications of the general theory of relativity*.

[97] Weinberg, S. (2008). *Cosmology, ISBN 9780198526827*. Oxford University Press Inc., New York.

[98] Zlatev, I., L. Wang, and P. J. Steinhardt (1999, Feb). Quintessence, cosmic coincidence, and the cosmological constant. *Phys. Rev. Lett. 82*, 896–899.